Petroleum Science 22 (2025) 4603–4623

Contents lists available at ScienceDirect

Petroleum Science

journal homepage: www.keaipublishing.com/en/journals/petroleum-science

Original Paper

A dynamic unified well-killing model for synergistic regulation of multiple well-killing methods

Hong-Wei Yang [a], Jun Li [a,b,*], Zhen-Yu Long [a], Xiu-Ling Zhang [a], Geng Zhang [a], Hui Zhang [a], Re-Yu Gao [c]

[a] China University of Petroleum-Beijing, Beijing, 102249, China
[b] China University of Petroleum-Beijing at Karamay, Karamay, 834000, Xinjiang, China
[c] CNPC Engineering Technology R & D Company Limited, Beijing, 102206, China

ARTICLE INFO

Article history:
Received 17 February 2025
Received in revised form
29 July 2025
Accepted 15 August 2025
Available online 22 August 2025

Edited by Jia-Jia Fei

Keywords:
Well-killing
Multi-method combination
Multiphase flow model
Standpipe and casing pressures
Shut-in

ABSTRACT

Ultra-deep and complex formations are characterized by narrow safety density windows and challenging well control. The combined use of multiple well-killing methods or temporary adjustments to well-killing strategies is becoming common. However, conventional well-killing models often struggle to calculate the parameters required for these special cases. In this paper, a boundary matrix for well-killing fluid density and volume is proposed to unify the driller's method, the engineer's method, and the weight-while-circulating method. Furthermore, a dynamic unified well-killing model is developed to enable the synergistic regulation of multiple well-killing methods. The model also can be applied with or without accounting for gas dissolution. Using this model, it is able to dynamically track key parameters during well killing and shut in the well at any time to determine the standpipe and casing pressures. The results indicate that the casing pressure drops to zero before the well-killing fluid returns to the annulus wellhead, and continued injection of the fluid leads to a gradual increase in standpipe pressure, a phenomenon not previously accounted for. The discrepancy between the actual and calculated standpipe/casing pressures after shut-in can be utilized to assess whether the downhole gas kick is effectively controlled. Through real-time adjustments to the boundary matrix, updated well-killing parameters can be derived for conventional method, multi-method combination, temporary strategy modification, and other well-killing scenarios. The model was applied to two field wells under water- and oil-based drilling fluids. No secondary downhole complications occurred during well killing, and the calculated pressure curves closely matched the measured construction pressure curves, confirming the model's reliability and applicability. This study provides valuable theoretical guidance for enhancing well control safety in ultra-deep and complex formations.

© 2025 The Authors. Publishing services by Elsevier B.V. on behalf of KeAi Communications Co. Ltd. This is an open access article under the CC BY-NC-ND license (http://creativecommons.org/licenses/by-nc-nd/4.0/).

* Corresponding author.
E-mail address: lijun446@vip.163.com (J. Li).
Peer review under the responsibility of China University of Petroleum (Beijing).

https://doi.org/10.1016/j.petsci.2025.08.025
1995-8226/© 2025 The Authors. Publishing services by Elsevier B.V. on behalf of KeAi Communications Co. Ltd. This is an open access article under the CC BY-NC-ND license (http://creativecommons.org/licenses/by-nc-nd/4.0/).

Nomenclature

A	wellbore cross-sectional area, m^2
A_e	distribution coefficient under bubble and slug flow
B_o	volume coefficient of drilling fluid
c_0	gas distribution coefficient
c_g	gas mass solubility, kg/kg
C_p	specific heat capacity, J/(kg·°C)
F	circulation pressure loss, Pa
g	gravitational acceleration, m/s^2
h	height of drilling fluid in the wellbore, m
h_c	convective heat transfer coefficient of the casing, W/(m^2·°C)
h_p	convective heat transfer coefficient of the drill pipe, W/(m^2·°C)
H_{depth}	wellbore length, m
P	wellbore pressure, Pa
q_{pump}	pump rate, m^3/s
r_{ci}	casing inner diameter, m
r_{co}	casing outer diameter, m
r_{pi}	drill pipe inner diameter, m
r_{po}	drill pipe outer diameter, m
R_g	saturated solubility, m3/m3
R_o	solubility of gas in oil-based drilling fluid, m^3/m^3
t	time, s
t_{bottom}	time for the well-killing fluid to reach the bottomhole, s
t_{top}	time for the well-killing fluid to return the annulus wellhead, s
T	temperature, °C
T_D	the dimensionless formation temperature equation
U	integrated convective heat transfer coefficient, W/(m^2·°C)
v	flow rate, m/s
v_c	characteristic velocity of gas, m/s
v_∞	gas slip velocity, m/s
V_a	annulus fluid volume, m^3
V_L	injected drilling fluid volume, m^3
V_p	volume of fluid in the drill string, m^3
V_{pit}	pit gain, m^3
z	axial distance, m
α	volume fraction
χ	decay term of the profile coefficient
ρ	density, kg/cm3
λ	thermal conductivity, W/(m·°C)
λ_c	thermal conductivity of the casing, W/(m·°C)
λ_{ce}	thermal conductivity of the cement ring, W/(m·°C)
θ	well inclination angle, rad

Subscripts

a	annulus
f	formation
i, j, k	$i, j, k = 0$ is the original drilling fluid, and $i, j, k = 1,2, \ldots, n$ is the well-killing fluid of the ith density
in	injection
g	gas phase
g,sc	gas phase under the standard conditions
L	liquid phase
n	the number drilling fluids with different densities
out	outflow
p	in the drill pipe

1. Introduction

In recent years, ultra-deep formations become primary targets for oil-gas exploration and development (He et al., 2023; Ma et al., 2022). These formations are characterized by high temperatures and pressures, complex pressure systems, developed fractures and cavities, and narrow safety density windows. These challenging conditions complicate wellbore pressure control and increase the risk of gas kicks (Li et al., 2016; Yang et al., 2024). Any failure may escalate into blowouts, endangering the safety of personnel, the environment, and economic outcomes.

Well-killing is a crucial technique for dealing with gas kick. The primary well-killing methods include the choke-while-circulating method (such as the engineer's method, driller's method, and weight-while-circulating method) and specialized method (including the bullheading method, displacement method, dynamic killing method, etc.) (Zhou et al., 2018; Chantose et al., 2018). In practical engineering applications, the choke-while-circulating method is capable of addressing over 85% of gas kicks and is the most important well-killing method. Therefore, this study focuses on the choke-while-circulating method.

The fundamental principle of the choke-while-circulating well-killing method is to maintain a constant bottomhole pressure that is slightly greater than the formation pore pressure. This constant bottomhole pressure is typically achieved by regulating standpipe or casing pressure in the field. Therefore, the accurate and well-founded design of standpipe and casing pressures during well killing is of critical importance. However, the wellbore flow state and pressure are complex due to various factors, such as the intricate gas-liquid two-phase flow, variations in drilling fluid properties under ultra-high temperature and pressure, and differing boundary conditions associated with various well-killing methods (Sun et al., 2017; Zhang et al., 2021). Consequently, many scholars conducted research on this issue.

Following a gas kick, the gas primarily flows in the annulus, with minimal or no gas entering the drill string. Consequently, the fluid in the drill string can be reasonably regarded as single-phase flow. In earlier stages, when the gas-liquid two-phase flow model was not fully developed, the standpipe pressure control method was widely employed for well-killing operations. This method involves determining the standpipe pressure during well killing based on the momentum conservation equation. Goins (1969) first formally proposed the standpipe pressure control method in 1969. Subsequently, researchers conducted many studies on the corresponding models under various well-killing methods, well types, and operational conditions (Letbetter, 1975; Holand, 2001; Noynaert and Schubert, 2005). This method remains the most commonly used in current field operations, demonstrating a high success rate and good adaptability in formations with a wide safety density window. However, in ultra-deep and complex formations, where the pressure system is sensitive and the safety density window is narrow, the success rate of this method significantly decreases, leading to elevated well control safety risks. The main limitation of standpipe pressure control method lies in its indirect nature.

If casing pressure can be accurately determined during well killing, it can be directly controlled to maintain constant bottomhole pressure. However, the presence of gas-liquid two-phase flow in the annulus makes casing pressure calculation difficult. With advancements in wellbore multiphase flow theory, extensive research was conducted on refining wellbore pressure descriptions for different

well-killing methods. The multiphase flow model treats the entire flow field as a continuum of interacting phases. For fluids in different phases, continuity, momentum conservation, and energy conservation equations are derived and solved simultaneously to capture phase interactions. The model is currently the most widely recognized analytical approach, providing detailed characteristic parameters for each phase of the flow. The representative studies on wellbore multiphase flow theory include: Orkiszewski method (Orkiszewski, 1967), Beggs-Brill method (Beggs and Brill, 1973), Hasan-Kabir method (Hasan and Kabir, 1988), Ansari method (Ansari et al., 1994) and so on. Based on these multiphase flow theories, typical studies of wellbore pressure calculations during gas kick and well killing are shown in Table 1.

The above analysis indicates that research on kick and well-killing simulation based on multiphase flow theory is extensive, covering various operating conditions, well types, kick fluids, drilling fluids, and drilling environments. However, most studies focus on conventional kick and well-killing scenarios, with limited specificity for different well-killing methods. While some studies have developed calculation models for the driller's method, the engineer's method, and the weight-while-circulating method, these models are independent and lack integration, making joint application challenging.

In ultra-deep and complex formations, gas kicks often result in challenges such as high standpipe or casing pressures and large gas fraction. The combined use of multiple well-killing methods or dynamic adjustments to well-killing strategies is becoming increasingly common. For instance, high-temperature and pressure conditions complicate the accurate evaluation of formation pore pressure, often requiring the joint application of multiple well-killing methods. In cases of high standpipe pressure, the killing fluid density may need to be gradually increased to prevent formation breakdown and more severe gas kick. Likewise, in formations where kick and mud loss coexist, large killing fluid loss may occur, necessitating temporary adjustments to well-killing parameters. However, existing studies fail to account for these scenarios and lack adaptability for calculating the relevant parameters.

This paper proposes a boundary matrix for the density and volume of killing fluid at the drill string inlet. Considering the effects of high temperature, high pressure, and gas dissolution, a dynamic unified well-killing model is developed for the synergistic regulation of multiple well-killing methods. The model integrates the driller's method, engineer's method, and weight-while-circulating method, enabling the calculation of key parameters and time node tracking in all choke-while-circulating well-killing scenarios. It provides a theoretical foundation for well-killing design in ultra-deep and complex formations.

2. The dynamic unified well-killing model

2.1. Physical model

Fig. 1 shows the dynamic well-killing processes of the engineer's method, the driller's method, and the weight-while-circulating method. These methods all involve removing formation-invaded gas from the annulus, with their primary distinction being the density of the well-killing fluid injected through the drill string inlet at different well-killing stages. The hydrostatic pressure varies during well killing across different well-killing methods. To balance formation pore pressure, a certain choke pressure needs to be controlled at the annulus wellhead. Therefore, simulating complex wellbore flow, tracking borehole parameter variations, and designing well-killing wellhead pressures are complex calculations. The use of oil-based drilling fluid increases this complexity due to gas dissolution and separation in the wellbore.

However, the actual well-killing is more complex, particularly in challenging formations where multiple methods are often combined for coordinated control. Additionally, problems such as mud loss, secondary gas kicks, or an imbalance between killing fluid and formation pore pressure may arise, necessitating adjustments to the well-killing strategy or parameters. However, existing well-killing models lack integration and real-time parameter adjustment capabilities, limiting their adaptability to the complex and ultra-deep well.

To address the above issues, a unified boundary condition is proposed to integrate the engineer's method, driller's method, and weight-while-circulating method. This boundary condition is expressed as a matrix of killing fluid density and volume. Combined with the wellbore multiphase flow theory, a calculation model is developed to determine key parameters for scenarios where different well-killing methods are used jointly or the strategy is adjusted temporarily. The assumptions of the model are as follows:

(1) As the gas dissolution in water-based drilling fluid is negligible, only its dissolution in oil-based drilling fluid is considered here.
(2) The gas and liquid at the same wellbore cross-section share identical pressure and temperature.
(3) Cuttings and drilling fluid in the wellbore are treated as a single mixed phase, with the migration of cuttings not considered separately.
(4) The shut-in process is ignored, and the gas kick volume during this period is calculated based on the final shut-in casing pressure prior to initiating well-killing.
(5) A check valve is generally installed in the downhole drill string, preventing consideration of gas invasion into the drill string.

2.2. Two-phase flow model for the gas-liquid mixture section in the annulus

From the onset of a gas kick to the complete removal of gas, a complex gas-liquid two-phase flow develops in the annulus, as illustrated in Fig. 1. In water-based drilling fluids, formation gas invades the wellbore, migrates to the annulus wellhead along with the drilling fluid, and gradually expands. In oil-based drilling fluids, the invading gas initially dissolves in the fluid and later transitions into free gas near the wellhead during migration (Thomas et al., 1984; Yin et al., 2024a). Of course, if the gas kick rate is large, not all gas in the lower wellbore will dissolve in the drilling fluid.

The drift flux model is widely used to simulate multiphase flow behavior in the wellbore, accounting for gas-liquid slip and gas fraction distribution across the flow cross-section. It offers relatively high accuracy with manageable computational complexity (Sun et al., 2017; Yang et al., 2020; Xu et al., 2021). Here a drift-flux-based model that incorporates both gas dissolution and non-dissolution scenarios develops.

Fig. 2 illustrates the simplified mass changes of each fluid phase within the control volume. Within the time interval dt, $A\alpha_i\rho_i v_i \mathrm{d}t$ is the mass of the gas or liquid flowing into the control volume; $A\alpha_L\rho_L c_g v_L \mathrm{d}t$ is the mass of the dissolved gas flowing into the control volume; $A\alpha_i\rho_i v_i \mathrm{d}t+\partial(A\alpha_i\rho_i v_i)/\partial z\ \mathrm{d}z\mathrm{d}t$ is the mass of the gas or liquid phase flowing out of the control volume; $A\alpha_L\rho_L c_g v_L \mathrm{d}t+\partial(A\alpha_L\rho_L c_g v_L)/\partial z\ \mathrm{d}z\mathrm{d}t$ is the mass of the dissolved gas flowing out of the control volume; $\partial(A\alpha_i\rho_i)/\partial t\ \mathrm{d}t\mathrm{d}z$ is the mass change of the gas or liquid; $\partial(A\alpha_L\rho_L c_g)/\partial t\ \mathrm{d}t\mathrm{d}z$ is the mass of the dissolved or released gas.

Based on the principle of mass conservation, the continuity equation for dissolved gas can be expressed as:

Table 1
Typical studies of wellbore pressure calculations during gas kick and well killing.

Author	Condition	Result
Nunes et al. (2002)	Kick	An analytical model, suitable for large gas kick volumes, was used to calculate the pressure and gas fraction in the annulus and choke line.
Santos et al. (2007)	Kick	The concept of void fraction was introduced, considering the effects of gas-liquid slip and frictional pressure losses in two-phase flow.
Meng et al. (2015), Wei et al. (2014, 2018), and Xu et al. (2015)	Kick	A wellbore gas-liquid two-phase flow model and numerical solution algorithm were developed to simulate variations in flow parameters during underbalanced drilling, gas drilling, and gas kick scenarios.
Thomas et al. (1984), Rommetveit et al. (1989), Monteiro et al. (2008), and Yin et al. (2022, 2024a)	Kick	(1) A transient multiphase flow model was developed, considering the effects of gas solubility and formation volume factor. (2) The impact of gas solubility in water-, oil-, and synthetic-based drilling fluids on gas kick monitoring indicators was analyzed.
Su et al. (2024)	Kick	A new transient flow model considering wellbore-formation coupling and gas solubility on flow behavior is developed to simulate gas kicks during horizontal drilling.
Yang et al. (2019a,b, 2020) and Xu et al. (2021)	Kick	(1) A transient gas-liquid two-phase flow model under non-isothermal conditions was developed, considering the effects of high temperature and high pressure in deep-formation and deep-water drilling. (2) The impact of unsteady interphase mass transfer on the wellbore flow state was also incorporated.
Yin et al. (2025)	Kick and shut-in	For excessive shut-in casing pressure, a multiphase flow model for pressure relief is established and a method is proposed to minimize the risk of gas kick recurrence during pressure relief.
Ju et al. (2022) and Yin et al. (2024b)	Kick and shut-in	(1) The complex nonlinear relationship between kick parameters and surface logging data was established. (2) The intelligent inversion method was used to obtain formation pressure and kick parameters.
Wang and Sun (2009), Sun et al. (2017, 2018a), Gao et al. (2017), and Sun et al. (2018b)	Kick and well-killing	(1) A set of control equations for multiphase and multi-component flow was developed, incorporating the effects of phase transitions in sour gas and natural gas hydrates. (2) Well-killing models for various methods were established, and the multiphase flow behaviors during gas kick and well-killing were analyzed.
Zhang et al. (2012)	Well-killing	(1) Well-killing models for various methods were established based on the characteristics of the driller's method and the engineer's method. (2) Factors such as the transient temperature field and the horizontal well were considered.
Feng et al. (2015, 2016)	Well killing	(1) A deepwater well-killing model was developed based on the driller's method, accounting for choke line friction and gas expansion. (2) A dynamic well-killing flow model was established, revealing wellbore pressure variation under variable pump rate and drilling fluid density conditions.
Yuan et al. (2015)	Well-killing	(1) For deepwater well-killing, the transient wellbore pressure variation was calculated accounting for choke line friction loss, U-tube effect, and fluid density changes. (2) The mud volume, pump rate, and minimum return time of killing fluid to the platform were also predicted.
Yin et al. (2023)	Kick and well-killing	The Y-shaped tube principle was proposed. Using the theory of well-killing fluid reflux and zero net liquid flow in the wellbore below the drill bit, a gas-liquid two-phase flow model was developed, the dynamic well-killing theory was established, and the variations in the well-killing parameters was revealed.
Zhang et al. (2022)	Well-killing	(1) The discrepancies between simulation data and real-time data from rig, seafloor, and bottomhole monitoring points under gas kick and well-killing were analyzed. (2) Using the real-time inversion method, an intelligent well-killing control approach was developed, driven by the coupling of simulation and real-time data.
Mao et al. (2025)	Well-killing	

Table 1 (*continued*)

Author	Condition	Result
		(1) For RMR (riserless mud recovery) system, the overflow control equation considering the lifting force of subsea pump is established. (2) The dynamic well control process of the RMR system after overflow under the two modes of constant subsea pump displacement and constant inlet pressure of subsea pump is simulated.
Davoudi et al. (2011), Johnson et al. (2017), Yang et al. (2022), and Vega et al. (2025)	Managed pressure well-killing	(1) To address gas kick in managed pressure drilling, dynamic control models were developed, incorporating gas dissolution, gas slippage, and temperature-pressure coupling under transient multi-phase flow conditions. (2) The response patterns of standpipe pressure, backpressure, choke opening, pit gain, and outlet flow rate in managed pressure drilling were analyzed. (3) The effectiveness of gas kick treatment under increased wellhead backpressure, increased flow rate, and combined backpressure-flow rate control was analyzed. (4) The application of dynamic or conventional circulation techniques was decided, considering factors such as predictions of pressure peaks, as well as intensity and volume of the kick.

$$A\alpha_L\rho_L c_g v_L \mathrm{d}t - \left[A\alpha_L\rho_L c_g v_L \mathrm{d}t + \frac{\partial(A\alpha_L\rho_L c_g v_L)\mathrm{d}z}{\partial z}\mathrm{d}t\right] = \frac{\partial(A\alpha_L\rho_L c_g)\mathrm{d}t}{\partial t}\mathrm{d}z \tag{1}$$

After simplification, it becomes:

$$\frac{\partial(A\alpha_L\rho_L c_g)}{\partial t} + \frac{\partial(A\alpha_L\rho_L c_g v_L)}{\partial z} = 0 \tag{2}$$

Similarly, the continuity equation for free gas can be expressed as:

$$\left(A\alpha_g\rho_g v_g \mathrm{d}t + A\alpha_L\rho_L c_g v_L \mathrm{d}t\right) - \left[\begin{array}{l}\left(A\alpha_g\rho_g v_g \mathrm{d}t + \frac{\partial(A\alpha_L\rho_L v_L)\mathrm{d}z}{\partial z}\mathrm{d}t\right) + \\ \left(A\alpha_L\rho_L c_g v_L \mathrm{d}t + \frac{\partial(A\alpha_L\rho_L c_g v_L)\mathrm{d}z}{\partial z}\mathrm{d}t\right)\end{array}\right] = \frac{\partial(A\alpha_g\rho_g)\mathrm{d}t}{\partial t}\mathrm{d}z - \frac{\partial(A\alpha_L\rho_L c_g)\mathrm{d}t}{\partial t}\mathrm{d}z \tag{3}$$

The simplification is as follows:

$$\frac{\partial(A\alpha_g\rho_g + A\alpha_L\rho_L c_g)}{\partial t} + \frac{\partial(A\alpha_g\rho_g v_g + A\alpha_L\rho_L c_g v_L)}{\partial z} = 0 \tag{4}$$

Similarly, the continuity equation for the liquid containing dissolved gas can be expressed as:

$$\left(A\alpha_L\rho_L v_L \mathrm{d}t + A\alpha_L\rho_L c_g v_L \mathrm{d}t\right) - \left[\begin{array}{l}\left(A\alpha_L\rho_L v_L \mathrm{d}t + \frac{\partial(A\alpha_L\rho_L v_L)\mathrm{d}z}{\partial z}\mathrm{d}t\right) + \\ \left(A\alpha_L\rho_L c_g v_L \mathrm{d}t + \frac{\partial(A\alpha_L\rho_L c_g v_L)\mathrm{d}z}{\partial z}\mathrm{d}t\right)\end{array}\right] = \frac{\partial(A\alpha_L\rho_L)\mathrm{d}t}{\partial t}\mathrm{d}z - \frac{\partial(A\alpha_L\rho_L c_g)\mathrm{d}t}{\partial t}\mathrm{d}z \tag{5}$$

After simplification, it is expressed as:

$$\frac{\partial(A\alpha_L\rho_L - A\alpha_L\rho_L c_g)}{\partial t} + \frac{\partial(A\alpha_L\rho_L v_L - A\alpha_L\rho_L c_g v_L)}{\partial z} = 0 \tag{6}$$

Treating the liquid, free gas, and dissolved gas as a mixed phase, the wellbore pressure change is described by the mixed momentum conservation equation:

$$\frac{\partial(A\alpha_g\rho_g v_g + A\alpha_L\rho_L v_L)}{\partial t} + \frac{\partial\left(A\alpha_g\rho_g v_g^2 + A\alpha_L\rho_L v_L^2\right)}{\partial z} + \frac{\partial(AP)}{\partial z} = -AF - A(\alpha_g\rho_g + \alpha_L\rho_L)g\cos\theta \tag{7}$$

Eqs. (4) and (6) actually reflect the effects of gas dissolution and separation on the mass of free gas and liquid. This process depends on the gas mass solubility c_g, which is a function of wellbore temperature and pressure. Meanwhile, wellbore temperature and pressure are also influenced by gas dissolution and evolution, forming a fully coupled process.

The gas solubility c_g, is related to the saturation solubility (R_g) of the oil-based drilling fluid. Previous research on R_g primarily falls into two categories. Most studies assume that the process of gas dissolution and evolution occurs instantaneously (White and Walton, 1990; Petersen et al., 2008; Ma et al., 2016; Yin et al., 2017; Nwaka et al., 2020). When $c_g < R_g$, the invading gas fully dissolves in the oil-based drilling fluid, with no free gas present. When $c_g > R_g$, the drilling fluid reaches saturation, and the undissolved gas exists as free gas. Other studies, based on experimental results, suggested that gas dissolution was a slower process and proposed unsteady interphase mass transfer models to capture this behavior (Grimstad et al., 2017; Bjørkevoll et al., 2018; Yang et al., 2020). However, the gas dissolution process is influenced by various factors, such as bubble morphology, slip rate, interfacial tension, flow state, two-phase flow pattern and so on. The complex wellbore multiphase flow makes it difficult to accurately characterize the unsteady interphase mass transfer rate. Consequently, this paper adopts the conventional approach used by most researchers, assuming that gas dissolution and separation occur instantaneously.

As mentioned above, when $c_g < R_g$, the gas fully dissolves in the oil-based drilling fluid, resulting in $\alpha_g = 0$. In this case, Eqs. (2) and (6) remain applicable as the continuity equations for dissolved gas and liquid, while the continuity equation for free gas is no longer required. The momentum conservation equation, Eq. (7), simplifies to:

$$\frac{\partial(A\alpha_L\rho_L v_L)}{\partial t} + \frac{\partial(A\alpha_L\rho_L v_L^2)}{\partial z} + \frac{\partial(AP)}{\partial z} = -AF - A\rho_L g\cos\theta \tag{8}$$

For water-based drilling fluid, gas dissolution is neglected ($c_g = 0$). Thus, the continuity equations for gas and liquid are simplified as follows:

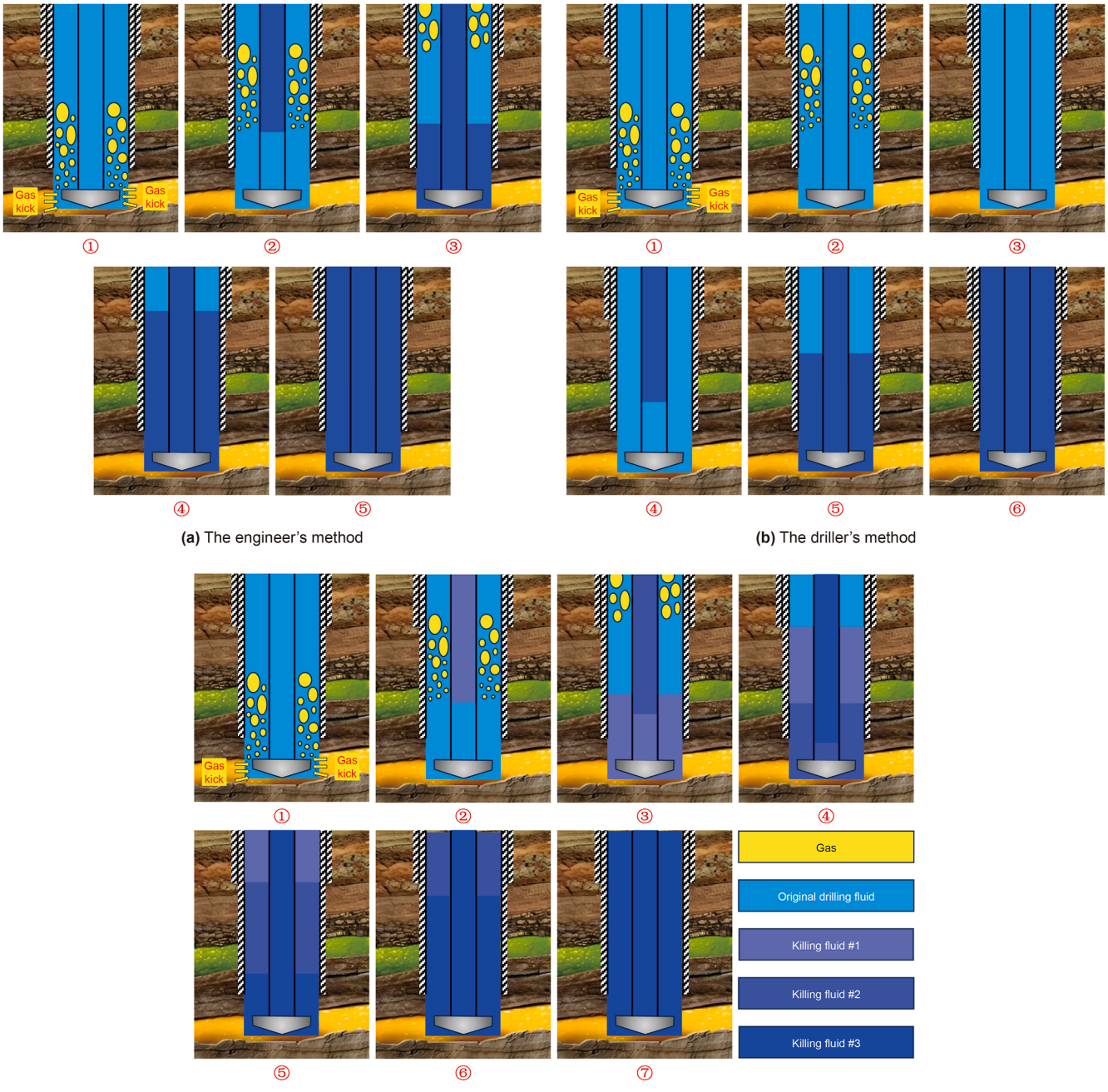

(a) The engineer's method

(b) The driller's method

(c) The weight-while-circulating method

Fig. 1. Schematic diagram of the dynamic well-killing process of different methods.

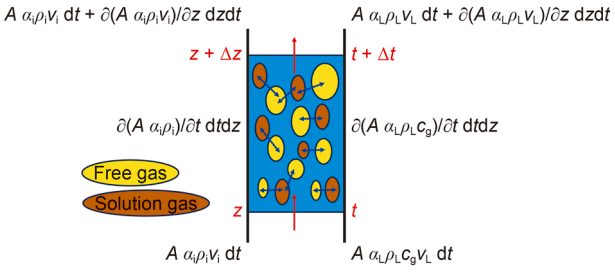

Fig. 2. A simplified schematic diagram of the mass change of each phase.

$$\frac{\partial(A\alpha_g\rho_g)}{\partial t}+\frac{\partial(A\alpha_g\rho_g v_g)}{\partial z}=0 \tag{9}$$

$$\frac{\partial(A\alpha_L\rho_L)}{\partial t}+\frac{\partial(A\alpha_L\rho_L v_L)}{\partial z}=0 \tag{10}$$

The momentum conservation equation for the gas-liquid mixture remains Eq. (7). The key difference is that the liquid contains no dissolved gas, and its density corresponds to that of the pure drilling fluid.

The gas-liquid interphase slip relationship is given by:

$$v_g = c_0(\alpha_g v_g + \alpha_L v_L) + v_\infty \tag{11}$$

In the gas-liquid interphase slip relationship described in Eq. (11), the gas distribution coefficient (c_0) and slip velocity (v_∞) depend on the gas-liquid two-phase flow patterns, which include dispersed bubble flow, bubble flow, slug flow, churn flow, and annular flow. Hasan and Kabir (1988) proposed equations to characterize c_0 and v_∞ under different flow patterns, using an integrated model with five piecewise functions. However, this model suffers from discontinuities during flow pattern transitions, often causing non-convergence in two-phase flow calculations. To address this problem, Shi et al. (2005) developed unified models for c_0 and v_∞ based on extensive experimental data from previous studies. This model was widely applied in simulating wellbore gas-liquid two-phase flow in the petroleum industry, with their applicability and reliability thoroughly validated. Therefore, Shi's model is adopted here to characterize the gas-liquid slip relationship.

The equation of the gas distribution coefficient (c_0) is:

$$c_0 = \frac{A_e}{1 + (A_e - 1)\chi^2} \tag{12}$$

The equation of the slip velocity (v_∞) is:

$$v_\infty = \frac{c_0 v_c (1 - \alpha_g c_0) K(\alpha_g)}{1 - \alpha_g c_0 \left(1 - (\rho_g/\rho_L)^{1/2}\right)} (\cos\theta)^{1/2} (1 + \sin\theta)^2 \tag{13}$$

2.3. Wellbore pressure model for the single-phase flow region

Except for the annulus gas-liquid mixing section, the drilling fluid flows as a single phase, as shown in Fig. 1. The fluid density and distribution within the single-phase flow region change dynamically during well killing, depending on the specific well-killing method used.

The wellbore pressure in the single-phase flow region can be expressed as:

$$\frac{\partial P}{\partial z} = -F - \sum_i \rho_{Li} g \cos\theta \tag{14}$$

where ρ_{Li} is the density of killing fluid, and the subscript i denotes the i-th killing fluid injected in sequence.

2.4. Unified boundary matrix and dynamic distribution of well-killing fluids

2.4.1. The boundary matrix of the unified model

The driller's method, the engineer's method, and the weight-while-circulating method are all categorized as choke-while-circulating well-killing techniques, sharing the same fundamental principle. Each method involves circulating and removing formation-invaded fluids by injecting new drilling fluid, thereby re-establishing a new pressure equilibrium between the wellbore and the formation. However, their operational processes differ, as shown in Fig. 1. Traditional calculation models for these methods were developed with a primary focus on their specific operational procedures, which makes it difficult to establish connections between the calculation models of different well-killing methods.

To adapt to the increasingly complex well-killing scenarios, a unified boundary matrix is proposed to integrate the three well-killing methods, enabling the unification of their calculation models. This unified boundary matrix is characterized by the densities and volumes of various well-killing fluids dynamically injected at the drill string inlet, as expressed in Eq. (15):

$$F(\rho_L, V_L) = \begin{bmatrix} \rho_{L1}, V_{L1} \\ \rho_{L2}, V_{L2} \\ \cdots \\ \rho_{L(n-1)}, V_{L(n-1)} \\ \rho_{Ln}, V_{Ln} \end{bmatrix} \tag{15}$$

This idea, which de-emphasizes the specifics of the well-killing operational procedures and focuses on the injection volumes of well-killing fluids with varying densities, aligns well with practical conditions. Moreover, it simplifies the calculations for different well-killing methods. The unified boundary matrix achieves the following: (1) Simulated calculations for the three well-killing methods individually; (2) Simulated calculations for scenarios involving combining multiple well-killing methods; (3) Simulated calculations for temporary adjustments to the well-killing strategy. The details are explained as follows:

For the engineer's method, a certain volume of well-killing fluid is directly injected to balance the formation pore pressure. The corresponding boundary matrix equation is expressed as:

$$F(\rho_L, V_L) = \begin{bmatrix} \rho_{L1}, V_{L1} \\ \rho_{L2}, 0 \\ \cdots \\ \rho_{L(n-1)}, 0 \\ \rho_{Ln}, 0 \end{bmatrix} \tag{16}$$

For the driller's method, the original drilling fluid is first injected to circulate the annulus formation-invaded gas out of the wellbore, followed by the injection of well-killing fluid to balance the formation pore pressure. The corresponding boundary matrix equation is expressed as:

$$F(\rho_L, V_L) = \begin{bmatrix} \rho_{L1}, V_{L1} \\ \rho_{L2}, V_{L2} \\ \rho_{L3}, 0 \\ \cdots \\ \rho_{L(n-1)}, 0 \\ \rho_{Ln}, 0 \end{bmatrix}, \rho_{L1} = \rho_{L0} \tag{17}$$

For the weight-while-circulating method, the densities of the injected well-killing fluids are gradually increased until the formation pore pressure is balanced. The number of density increments and the volume of well-killing fluid at each density are determined based on the actual site conditions. The corresponding boundary matrix equation is expressed as:

$$F(\rho_L, V_L) = \begin{bmatrix} \rho_{L1}, V_{L1} \\ \rho_{L2}, V_{L2} \\ \rho_{L3}, V_{L3} \\ \rho_{L4}, V_{L4} \\ \cdots \\ \rho_{L(n-1)}, 0 \\ \rho_{Ln}, 0 \end{bmatrix} \tag{18}$$

For some complex gas kick scenarios, such as those involving large gas fraction, high standpipe and casing pressures, and difficulty in accurately determining formation pore pressure, well-killing operations become highly challenging and often require the combined use of different well-killing methods. A commonly approach includes the following steps: (1) Engineer's method: initially used to quickly reduce high casing pressure. (2) Driller's method: subsequently employed to accurately determine formation pore pressure and design the appropriate final well-killing fluid density. (3) Weight-while-circulating method: finally used to gradually inject well-

killing fluids and avoid the risk of mud loss that could occur with direct use of the final-density well-killing fluid, completing the well-killing. Additionally, other combined uses of well-killing methods may also arise in different situations. Eq. (18) can still characterize the boundary matrix, but the fluid densities (ρ_{L1}, ρ_{L2}, ρ_{L3}, …) do not necessarily increase progressively, as in the weight-while-circulating method. Another critical consideration is the reasonable design of the volumes for different well-killing fluids, which must be determined comprehensively based on actual conditions.

In the event of complications during well-killing, such as mud loss, secondary gas kicks, insufficient well-killing fluid volume, or fluid density failing to balance formation pore pressure, the well-killing strategy must be temporarily adjusted. In such cases, the subsequent well-killing process needs to be recalculated based on the current conditions. Consequently, the initially designed boundary matrix, Eq. (15), is expanded to form a new boundary matrix, as expressed in Eq. (19):

$$F(\rho_L, V_L) = \begin{bmatrix} \rho_{L1}, V_{L1} \\ \rho_{L2}, V_{L2} \\ \cdots \\ \rho_{L(n-1)}, V_{L(n-1)} \\ \rho_{Ln}, V_{Ln} \\ \rho_{L(n+1)}, V_{L(n+1)} \\ \rho_{L(n+2)}, V_{L(n+2)} \\ \cdots \end{bmatrix} \tag{19}$$

2.4.2. Dynamic distribution of well-killing fluids

During well killing, the dynamic migration of fluids with varying densities in the wellbore impacts the pressure profile. Consequently, it is essential for on-site engineers to monitor the dynamic changes in wellbore parameters and identify critical time points by tracking the movement of well-killing fluids of different densities. There are various scenarios for the well-killing fluid flow in the wellbore.

(1) In the drill string

The time for the well-killing fluid to reach the bottomhole from the inlet of the drill string is:

$$t_{bottom} = \frac{V_p}{q_{pump}} \tag{20}$$

① $t \le t_{bottom}$

When the well-killing fluid does not reach the bottomhole (i.e., $t \le t_{bottom}$), the volume of well-killing fluid injected into the drill string is:

$$V_{p,in}(t) = q_{pump} t \tag{21}$$

- When the well-killing fluid with a density of ρ_{L1} is being injected into the drill string inlet (i.e., $V_{p,in}(t) \le V_{L1}$), the length of the well-killing fluid with density of ρ_{L1} inside the drill string is:

$$h_{p,L1} = \frac{V_{p,in}(t)}{A_p} \tag{22}$$

The fluid density distribution inside the drill string is given by:

$$\rho_p = \begin{cases} \rho_{L1}, & h \le h_{p,L1} \\ \rho_{L0}, & h > h_{p,L1} \end{cases} \tag{23}$$

- When the well-killing fluid with a density of ρ_{Lj} is being injected into the drill string inlet (i.e., $\sum_{i=1}^{j-1} V_{Li} < V_{p,in}(t) \le \sum_{i=1}^{j} V_{Li}$, $j = 2, 3, \ldots, n$), the lengths of the well-killing fluids with densities of ρ_{L1}, ρ_{L2}, …, ρ_{Lj} inside the drill string are:

$$\begin{cases} h_{p,Li} = \dfrac{V_{Li}}{A_p}, i = 1, 2, \ldots, j-1 \\ h_{p,Li} = \dfrac{V_{p,in}(t) - \sum_{i=1}^{j-1} V_{Li}}{A_p}, i = j \end{cases} \tag{24}$$

The fluid densities distribution inside the drill string is:

$$\rho_p = \begin{cases} \rho_{Lj}, & h \le h_{p,Lj} \\ \rho_{Li}, & \sum_{m=i+1}^{j} h_{p,Lm} < h \le \sum_{m=i}^{j} h_{p,Lm}, \quad i = 1, 2, \ldots, j-1 \\ \rho_{L0}, & h > \sum_{i=1}^{j} h_{p,Li} \end{cases} \tag{25}$$

② $t > t_{bottom}$

When the well-killing fluid reaches the bottomhole (i.e., $t > t_{bottom}$), the volume of the fluid entering the annulus from the drill string is:

$$V_{p,out}(t) = q_{pump}(t - t_{tottom}) \tag{26}$$

- When the well-killing fluid with a density of ρ_{L1} is still being injected into the drill string inlet (i.e., $V_{p,in}(t) \le V_{L1}$), the length of the fluid with density of ρ_{L1} inside the drill string is:

$$h_{p,L1} = H_{depth} \tag{27}$$

The fluid densities distribution inside the drill string is:

$$\rho_p = \rho_{L1} \tag{28}$$

- When the well-killing fluid with a density of ρ_{Lj} is being injected into the drill string inlet, and the fluid with a density of ρ_{L1} is entering the annulus from the drill string (i.e., $\sum_{i=1}^{j-1} V_{Li} < V_{p,in}(t) \le \sum_{i=1}^{j} V_{Li}, j = 2, 3, \ldots, n$, and $V_{p,out}(t) \le V_{L1}$), the lengths of the well-killing fluids with densities of ρ_{L1}, ρ_{L2}, …, ρ_{Lj} within the drill string are:

$$\begin{cases} h_{p,L1} = \dfrac{V_{L1} - V_{p,out}(t)}{A_p} \\ h_{p,Li} = \dfrac{V_{Li}}{A_p}, i = 1, 2, ..., j-1 \\ h_{p,Lj} = H_{depth} - \sum_{i=1}^{j-1} h_{p,Li} \end{cases} \tag{29}$$

The fluid density distribution inside the drill string is:

$$\rho_p = \begin{cases} \rho_{Lj}, & h \le h_{p,Lj} \\ \rho_{Li}, & \sum_{m=i+1}^{j} h_{p,Lm} < h \le \sum_{m=i}^{j} h_{p,Lm}, \quad i = 2, 3, ..., j-1 \\ \rho_{L1}, & h > \sum_{i=2}^{j} h_{p,Li} \end{cases} \tag{30}$$

- When the well-killing fluid with a density of ρ_{Lj} is being injected into the drill string inlet, and the fluid with a density of ρ_{Lk} is entering the annulus from the drill string (i.e., $\sum_{i=1}^{j-1} V_{Li} < V_{p,in}(t) \le \sum_{i=1}^{j} V_{Li}$, $j = 2, 3, \ldots, n$, and $\sum_{i=1}^{k-1} V_{Li} < V_{p,out}(t) \le \sum_{i=1}^{k} V_{Li}, k = 2, 3, \ldots, j-1$), the lengths of the well-killing fluids with densities of ρ_{L1}, ρ_{L2}, …, ρ_{Lj} within the drill string are:

$$\begin{cases} h_{p,Li} = 0, i = 1, 2, ..., k-1 \\ h_{p,Li} = \dfrac{\sum_{m=1}^{i} V_{Lm} - V_{p,out}(t)}{A_p}, i = k \\ h_{p,Li} = \dfrac{V_{Li}}{A_p}, i = k+1, k+2, ..., j-1 \\ h_{p,Li} = H_{depth} - \sum_{i=k}^{j-1} h_{p,Li}, i = j \end{cases} \tag{31}$$

The fluid density distribution inside the drill string is:

$$\rho_p = \begin{cases} \rho_{Lj}, & h \le h_{p,Lj} \\ \rho_{Li}, & \sum_{m=i+1}^{j} h_{p,Lm} < h \le \sum_{m=i}^{j} h_{p,Lm}, \quad i = k+1, k+2 ..., j-1 \\ \rho_{Lk}, & h > \sum_{i=k+1}^{j} h_{p,Li} \end{cases} \tag{32}$$

- When the well-killing fluid with a density of ρ_{Lj} is being injected into the drill string inlet, and the fluid with a density of ρ_{Ln} is entering the annulus from the drill string (i.e., $\sum_{i=1}^{j-1} V_{Li} < V_{p,in}(t) \le \sum_{i=1}^{j} V_{Li}$, $j = 2, 3, \ldots, n$, and $\sum_{j=1}^{n-1} V_{Lj} < V_{p,out}(t) \le \sum_{j=1}^{n} V_{Lj}$), the lengths of the well-killing fluids with densities of ρ_{L1}, ρ_{L2}, …, ρ_{Ln} within the drill string are:

$$\begin{cases} h_{p,Lj} = 0, j = 1, 2, ..., n-1 \\ h_{p,Lj} = H_{depth}, j = n \end{cases} \tag{33}$$

The fluid density distribution inside the drill string is:

$$\rho_p = \rho_{Ln} \tag{34}$$

(2) In the annulus

The time required for the well-killing fluid to travel from the drill string inlet to the bottomhole and return to the annulus outlet is:

$$t_{top} = \frac{V_p + V_a}{q_{pump}} \tag{35}$$

① $t \le t_{bottom}$

When the well-killing fluid in the drill string does not reach the bottomhole (i.e., $t \le t_{bottom}$), the density profile of the liquid phase in the annulus is:

$$\rho_a = \rho_{L0} \tag{36}$$

② $t_{bottom} < t \le t_{top}$

When the well-killing fluid in the drill string reaches the bottomhole but has not yet returned to the annulus wellhead (i.e., $t_{bottom} < t \le t_{top}$), the volume of the well-killing fluid entering the annulus is equal to that of the well-killing fluid flowing out of the drill string.

$$V_{a,in}(t) = V_{p,out}(t) = q_{pump}(t - t_{tottom}) \tag{37}$$

- When the well-killing fluid with a density of ρ_{L1} is entering the annulus from the drill string (i.e., $V_{a,in}(t) \le V_{L1}$), the length of the well-killing fluid with a density of ρ_{L1} in the annulus is:

$$h_{a,L1} = \frac{V_{a,in}(t)}{A_a} \tag{38}$$

The density distribution of the liquid phase in the annulus is:

$$\rho_a = \begin{cases} \rho_{L0}, h \le H_{depth} - h_{a,L1} \\ \rho_{L1}, h > H_{depth} - h_{a,L1} \end{cases} \tag{39}$$

- When the well-killing fluid with a density of ρ_{Lj} is entering the annulus from the drill string (i.e., $\sum_{i=1}^{j-1} V_{Li} < V_{a,in}(t) \le \sum_{i=1}^{j} V_{Li}$, $j = 2, 3, \ldots, n$), the lengths of the well-killing fluids with densities of $\rho_{L1}, \rho_{L2}, \ldots, \rho_{Lj}$ in the annulus are:

$$\begin{cases} h_{a,Li} = \dfrac{V_{Li}}{A_a}, i = 1, 2, ..., j-1 \\ h_{a,Li} = \dfrac{V_{a,in}(t) - \sum_{i=1}^{j-1} V_{Li}}{A_a}, i = j \end{cases} \tag{40}$$

The density distribution of the liquid phase in the annulus is:

③ $t > t_{top}$

$$\rho_a = \begin{cases} \rho_{L0}, & h \le H_{depth} - \sum_{i=1}^{j} h_{a,Li} \\ \rho_{Li}, & H_{depth} - \sum_{m=i}^{j} h_{a,Lm} < h \le H_{depth} - \sum_{m=i+1}^{j} h_{a,Lm}, \quad i = 1, 2, ..., j-1 \\ \rho_{Lj}, & h > H_{depth} - h_{a,Lj} \end{cases} \tag{41}$$

Once the well-killing fluid begins to flow from the annulus wellhead (i.e., $t > t_{top}$), the discharged fluid volume is given by:

$$V_{a,out}(t) = q_{pump}(t - t_{top}) \tag{42}$$

- When the well-killing fluid with a density of ρ_{L1} is still entering the annulus from the drill string (i.e., $V_{a,in}(t) \le V_{L1}$), the length of the well-killing fluid with a density of ρ_{L1} in the annulus is:

$$h_{a,L1} = H_{depth} \tag{43}$$

The density distribution of the liquid phase in the annulus is:

$$\rho_a = \rho_{L1} \tag{44}$$

- When the well-killing fluid with a density of ρ_{Lj} is entering the annulus from the drill string and the well-killing fluid with a density of ρ_{L1} is flowing out of the annulus wellhead (i.e., $\sum_{i=1}^{j-1} V_{Li} < V_{a,in}(t) \le \sum_{i=1}^{j} V_{Li}, j = 2, 3, \ldots, n$, and $V_{a,out}(t) \le V_{L1}$), the lengths of the well-killing fluids with densities of $\rho_{L1}, \rho_{L2}, \ldots, \rho_{Lj}$ in the annulus are:

$$\begin{cases} h_{a,L1} = \dfrac{V_{L1} - V_{a,out}(t)}{A_a} \\ h_{a,Li} = \dfrac{V_{Li}}{A_a}, i = 1, 2, ..., j-1 \\ h_{a,Lj} = H_{depth} - \sum_{i=1}^{j-1} h_{a,Li} \end{cases} \tag{45}$$

The density distribution of the liquid phase in the annulus is

$$\rho_a = \begin{cases} \rho_{L1}, & h \le H_{depth} - \sum_{i=2}^{j} h_{a,Li} \\ \rho_{Li}, & H_{depth} - \sum_{m=i}^{j} h_{a,Lm} < h \le H_{depth} - \sum_{m=i+1}^{j} h_{a,Lm}, \quad i = 2, 3, ..., j-1 \\ \rho_{Lj}, & h > H_{depth} - h_{a,Lj} \end{cases} \tag{46}$$

- When the well-killing fluid with a density of ρ_{Lj} is entering the annulus from the drill string and the well-killing fluid with a density of ρ_{Lk} is flowing out of the annulus wellhead (i.e., $\sum_{i=1}^{j-1} V_{Li} < V_{a,in}(t) \le \sum_{i=1}^{j} V_{Li}$, $j = 2, 3, \ldots, n$, and $\sum_{i=1}^{k-1} V_{Li} < V_{a,out}(t) \le \sum_{i=1}^{k} V_{Li}$, $k = 2, 3, \ldots, j-1$), the lengths of the well-killing fluids with densities of $\rho_{L1}, \rho_{L2}, \ldots, \rho_{Lj}$ in the annulus are::

$$\begin{cases} h_{a,Li} = 0, i = 1, 2, \ldots, k-1 \\ h_{a,Li} = \dfrac{\sum_{m=1}^{i} V_{Lm} - V_{a,out}(t)}{A_a}, i = k \\ h_{a,Li} = \dfrac{V_{Li}}{A_a}, i = k+1, k+2, \ldots, j-1 \\ h_{a,Li} = H_{depth} - \sum_{i=k}^{j-1} h_{a,Li}, i = j \end{cases} \tag{47}$$

The density distribution of the liquid phase in the annulus is:

$$\rho_a = \begin{cases} \rho_{Lk}, & h \le H_{depth} - \sum_{i=k+1}^{j} h_{a,Li} \\ \rho_{Li}, & H_{depth} - \sum_{m=i}^{j} h_{a,Lm} < h \le H_{depth} - \sum_{m=i+1}^{j} h_{a,Lm}, \quad i = k+1, k+2 \ldots, j-1 \\ \rho_{Lj}, & h > H_{depth} - h_{a,Lj} \end{cases} \tag{48}$$

- When the well-killing fluid with a density of ρ_{Lj} is entering the annulus from the drill string and the well-killing fluid with a density of ρ_{Ln} is flowing out of the annulus wellhead (i.e., $\sum_{i=1}^{j-1} V_{Li} < V_{a,in}(t) \le \sum_{i=1}^{j} V_{Li}$, $j = 2, 3, \ldots, n$, and $\sum_{j=1}^{n-1} V_{Lj} < V_{a,out}(t) \le \sum_{j=1}^{n} V_{Lj}$), the lengths of the well-killing fluids with densities of $\rho_{L1}, \rho_{L2}, \ldots, \rho_{Lj}$ in the annulus are:

$$\begin{cases} h_{a,Lj} = 0, j = 1, 2, \ldots, n-1 \\ h_{a,Lj} = H_{depth}, j = n \end{cases} \tag{49}$$

The density distribution of the liquid phase in the annulus is:

$$\rho_a = \rho_{Ln} \tag{50}$$

2.5. Transient heat transfer model between wellbore and formation

Previous studies indicate that the wellbore and formation form a complex heat exchange system during drilling fluid circulation. Many research was conducted on this topic (Espinosa-Paredes and Espinosa-Martínez, 2009; Yang et al., 2015, 2019b). Based on the energy conservation equation, the transient heat transfer model for annulus fluid is expressed as:

$$\left(A\rho_g\alpha_g C_{pg} + A\rho_L\alpha_L C_{pL}\right)\frac{\partial T_a}{\partial t} + \left(\alpha_g v_g + \alpha_L v_L\right)\frac{\partial T_a}{\partial z} = \frac{T_f - T_a}{A_0} + \frac{T_p - T_a}{B_0} \tag{51}$$

where,

$$A_0 = \frac{1}{2\pi}\left(\frac{\lambda_f + r_{ci}U_a T_D}{r_{ci}U_a\lambda_f}\right) \tag{52}$$

$$B_0 = \frac{1}{2\pi r_{pi}U_p} \tag{53}$$

$$U_a^{-1} = \frac{r_{co}}{r_{ci}h_c} + \frac{r_{co}}{\lambda_c \ln(r_{co}/r_{ci})} + \frac{1}{\lambda_{ce}\ln(r_b/r_{co})} \tag{54}$$

$$U_p^{-1} = \frac{r_{po}}{r_{pi}h_p} + \frac{r_{po}}{\lambda_p \ln\left(r_{po}/r_{pi}\right)} + \frac{1}{h_p} \tag{55}$$

When the gas in the annulus is fully removed ($\alpha_g = 0$), Eq. (50) can be used to calculate the temperature changes for single-phase flow in the annulus.

Based on the energy conservation equation, the transient heat transfer model for fluid in the drill string is:

$$A\rho_L C_{pL}\frac{\partial T_p}{\partial t} + v_L\frac{\partial T_p}{\partial z} = -\frac{T_p - T_f}{B_0} \tag{56}$$

2.6. Auxiliary equation

Gas solubility is a critical parameter influencing the free gas fraction and wellbore pressure. Typically, gas solubility is calculated using either the equation of state method or the empirical formula method. The equation of state method requires satisfying phase equilibrium relationships and involves numerous iterative calculations. This approach also requires detailed information about the gas and drilling fluid components, making it complex and time-consuming. In contrast, the empirical formula method is much simpler and widely used. O'bryan (1998) proposed a widely accepted empirical formula for gas solubility based on experimental tests, as follows:

$$R_o = \left(\frac{P}{\eta T^{\xi}}\right)^{\zeta} \tag{57}$$

where, η, ξ, and ζ are coefficients determined by fitting experimental data. Due to the limited experimental dataset used by O'bryan (1998), the calculation error of Eq. (56) is as high as 24.1%. To improve accuracy in calculating gas solubility in oil-based drilling fluids, Sun et al. (2019) compiled a comprehensive experimental database from various studies. Using the least squares method, they determined the coefficients η, ξ, and ζ as 11.773, 0.122, and 1.29, respectively. They further conducted gas solubility experiments in oil-based drilling fluids and compared the model's calculations with experimental results. The error of

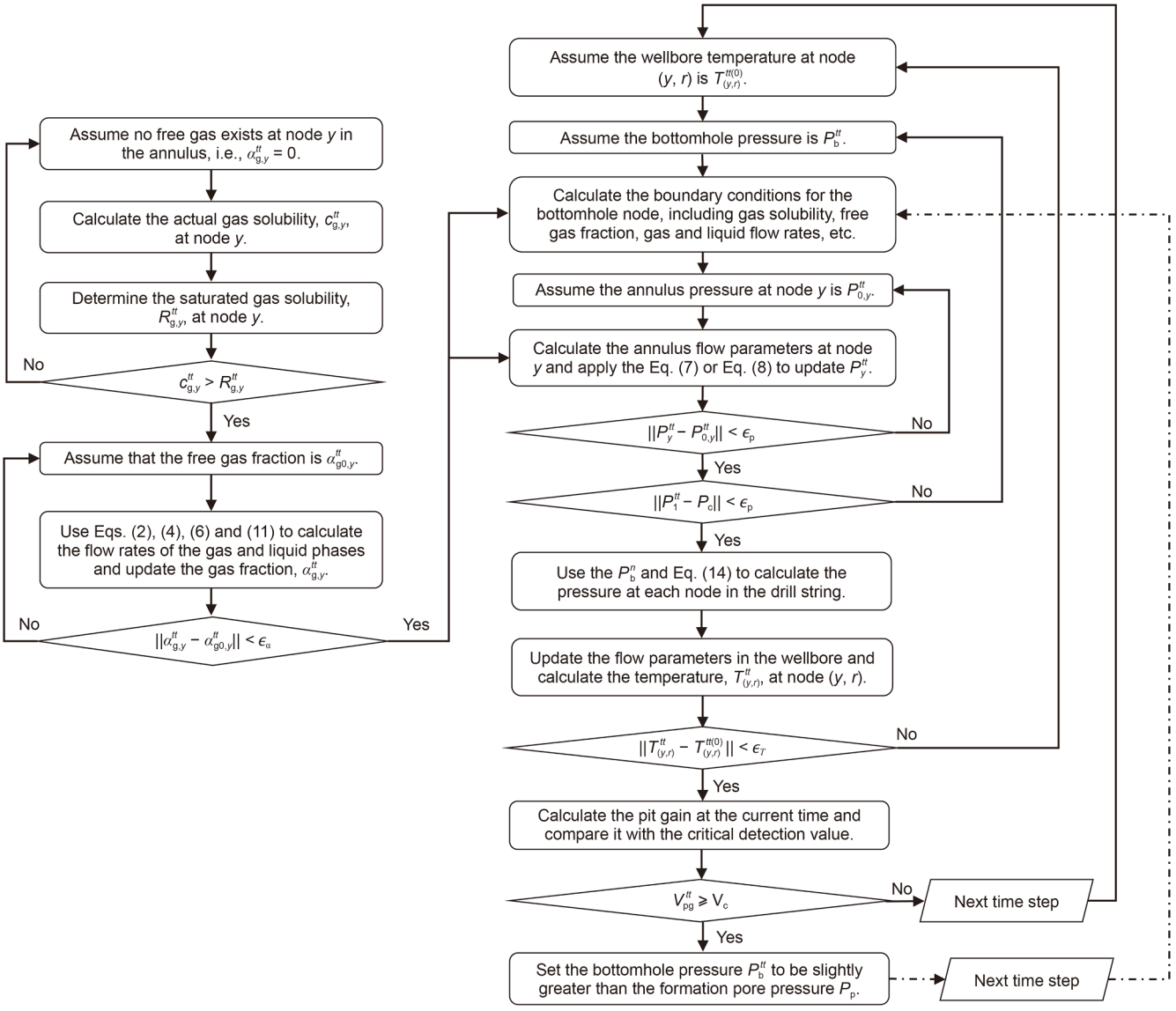

Fig. 3. The overall calculation flow.

the updated model was reduced to 8.06%. Therefore, the improved model developed by Sun et al. (2019) is adopted here.

The volume factor of oil-based drilling fluid can be expressed as:

$$B_o = 0.972 + 0.000147\left(\frac{R_o}{0.1781}\left(\frac{SG_g}{SG_L}\right)^{0.5} + 1.25[1.8(T-273.15)+32]\right)^{1.175} \tag{58}$$

Based on the volume factor of oil-based drilling fluid, the density of the fluid containing dissolved gas is calculated as:

$$\rho^*_L = \frac{\rho_L + R_o\rho_{g,sc}}{B_o} \tag{59}$$

Considering the expansion characteristics of oil-based drilling fluid with dissolved gas, the pit gain is expressed as:

$$V_{pit} = [(B_o - B_L)(1-\alpha_g) + \alpha_g]Az \tag{60}$$

3. Model solution

3.1. Model discretization

The hydraulic and thermodynamic models described above can be discretized and solved using the finite difference method. Both models can be represented in a unified form as:

$$\frac{\partial W_x}{\partial t} + \frac{\partial F_x(W_x)}{\partial z} = Q_x(W_x), \quad x = 1, 2, ..., 6 \tag{61}$$

In the hydraulics model, W_x, $F_x(W_x)$, and $Q_x(W_x)$ (x = 1,2, …,6) are functions of phase fraction, density, flow rate, gas solubility, and pressure. In the thermodynamic model, they are functions of temperature, as summarized in Table 2.

To enhance the stability of the solution process, the pressure term (P) in $F_4(W_4)$ is isolated to form $F^*_4(W_4)$. This allows the use of different discrete formats for $A\alpha_g\rho_g v_g^2 + A\alpha_L\rho_L v_L^2$ and P, respectively (Nickens, 1987). Using the finite difference method, the nonlinear partial differential equations for hydraulics and thermodynamics are discretized as:

Table 2
Variables in Eq. (60).

W_x	$F_x(W_x)$	$Q_x(W_x)$
$W_1 = A\alpha_L\rho_L c_g$	$F_1(W_1) = A\alpha_L\rho_L c_g v_L$	$Q_1(W_1) = 0$
$W_2 = A\alpha_g\rho_g + A\alpha_L\rho_L c_g$	$F_2(W_2) = A\alpha_g\rho_g v_g + A\alpha_L\rho_L c_g v_L$	$Q_2(W_2) = 0$
$W_3 = A\alpha_L\rho_L - A\alpha_L\rho_L c_g$	$F_3(W_3) = A\alpha_L\rho_L v_L - A\alpha_L\rho_L c_g v_L$	$Q_3(W_3) = 0$
$W_4 = A\alpha_g\rho_g v_g + A\alpha_L\rho_L v_L$	$F_4(W_4) = A\alpha_g\rho_g v_g^2 + A\alpha_L\rho_L v_L^2 + P$	$Q_4(W_4) = -AF - A(\alpha_g\rho_g + \alpha_L\rho_L)g\cos\theta$
	$F_4^*(W_4) = A\alpha_g\rho_g v_g^2 + A\alpha_L\rho_L v_L^2$	
$W_5 = (A\alpha_g\rho_g C_{pg} + A\alpha_L\rho_L C_{pL})T$	$F_5(W_5) = (\alpha_g v_g + \alpha_L v_L)T$	$Q_5(W_5) = \frac{T_f - T}{A_0} + \frac{T_p - T}{B_0}$
$W_6 = A\rho_L C_{pL} T$	$F_6(W_6) = v_L T$	$Q_6(W_6) = \frac{T_p - T}{B_0}$

Table 3
Basic parameters of the simulated well.

Parameter	Value	Parameter	Value
Well depth, m	7109	Original drilling fluid density, kg/m^3	1740
Casing length, m	6600	Original drilling fluid viscosity, Pa·s	0.038
Casing inner diameter, m	0.206	Original pump rate, m^3/s	0.018
Bit diameter, m	0.168	Well-killing pump rate, m^3/s	0.012
Drillpipe inner diameter, m	0.975	Shut-in casing pressure, MPa	6.64
Drillpipe outer diameter, m	0.114	Shut-in standpipe pressure, MPa	4.2

$$\frac{W_x|_{y+1/2}^{tt+1} - W_x|_{y+1/2}^{tt}}{\Delta t} + \frac{F_x(W_x)|_{y+1}^{tt+1} - F_x(W_x)|_{y}^{tt+1}}{\Delta z} = Q_x(W_x)|_{y+1/2}^{tt+1/2}, \quad x = 1,2,3 \tag{62}$$

$$\frac{W_x|_{y+1/2}^{tt+1} - W_x|_{y+1/2}^{tt}}{\Delta t} + \frac{F_x^*(W_x)|_{y+1}^{tt+1/2} - F_x^*(W_x)|_{y}^{tt+1/2}}{\Delta z} + \frac{(P)|_{y+1}^{tt+1} - (P)|_{y}^{tt+1}}{\Delta z} = Q_x(W_x)|_{y+1/2}^{tt+1/2}, \quad x = 4 \tag{63}$$

$$\frac{W_x|_{y+1}^{tt+1} - W_x|_{y+1}^{tt}}{\Delta t} + \frac{F_x(W_x)|_{y+1}^{tt+1} - F_x(W_x)|_{y}^{tt+1}}{\Delta z} = Q_x(W_x)|_{y+1}^{tt+1/2}, \quad x = 5,6 \tag{64}$$

where, $W|_{y+1/2} = \frac{W|_y + W|_{y+1}}{2}$, $W|^{tt+1/2} = \frac{W|^{tt} + W|^{tt+1}}{2}$, $W|_{y+1/2}^{tt+1/2} = \frac{W|_y^{tt} + W|_{y+1}^{tt} + W|_y^{tt+1} + W|_{y+1}^{tt+1}}{4}$.

3.2. Calculation procedure

Using the above models and applying the control principle of maintaining constant bottomhole pressure (slightly exceeding the formation pore pressure), the flow parameters and pressure variations during gas kick and well killing under different conditions can be calculated.

3.2.1. Gas solubility calculation procedure

(1) Initial assumption: Assume no free gas exists at node y in the annulus, i.e., $\alpha_{g,y}^{tt} = 0$.
(2) Calculate actual gas solubility: Use the gas mass conservation equation to calculate the actual gas solubility, $c_{g,y}^{tt}$, at node y.
(3) Compare with saturation: Determine the saturated gas solubility, $R_{g,y}^{tt}$, at node y. If $c_{g,y}^{tt} > R_{g,y}^{tt}$, free gas is present at node y, and the assumption in step (1) is incorrect. Proceed to step (4). If $c_{g,y}^{tt} \le R_{g,y}^{tt}$, the assumption in step (1) is valid. The gas solubility is equal to the actual solubility, $c_{g,y}^{tt}$, and the free gas fraction $\alpha_{g,y}^{tt} = 0$.
(4) Free gas fraction assumption: The oil-based drilling fluid at node y reaches saturation, i.e., $c_{g,y}^{tt} = R_{g,y}^{tt}$. Assume that the free gas fraction is $\alpha_{g0,y}^{tt}$.
(5) Update flow parameters: Use the gas and liquid mass conservation equations to calculate the flow rates of the gas and liquid phases. Update the gas fraction, $\alpha_{g,y}^{tt}$, based on the interphase slip relationship.
(6) Convergence check: Compare whether $||\alpha_{g,y}^{tt} - \alpha_{g0,y}^{tt}| < \varepsilon_\alpha$ is established. If this condition is met, the free gas fraction at node j is $\alpha_{g,y}^{tt}$; if not, return to step (4) and iterate.

3.2.2. Gas kick and well-killing parameter calculation procedure

(1) Initialize node conditions: Assume the temperature at node (y,r) in the wellbore is $T_{(y,r)}^{t(0)}$, and the bottomhole pressure is P_b^{tt}.
(2) Calculate bottomhole boundary conditions: Use the mass conservation equation and gas solubility model to

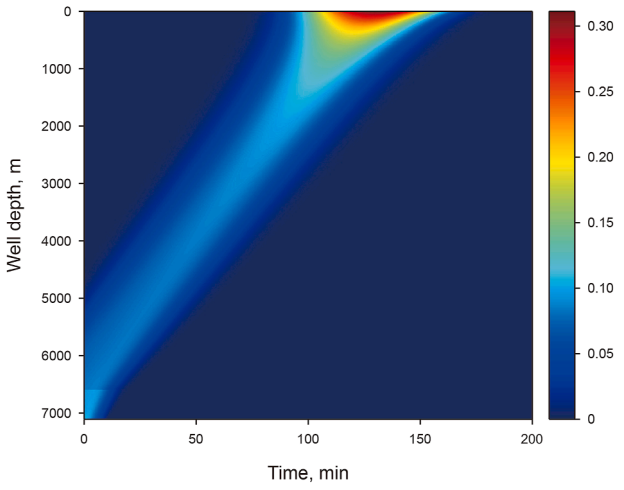

Fig. 4. Annulus gas migration in the water-based drilling fluid.

determine the boundary conditions for the bottomhole node, including gas kick rate, gas solubility, free gas fraction, gas and liquid densities, and gas and liquid flow rates.

(3) Assume annulus pressure: Assume the annulus pressure at node y is $P_{0,y}^{tt}$.

(4) Calculate annulus multiphase flow parameters: Using the mass conservation equation and gas solubility model, calculate the multiphase flow parameters at node y in the annulus.

(5) Update annulus pressure: Apply the momentum conservation equation in the annulus to update P_y^{tt} using the parameters at node y. Compare whether $\left\|P_y^{tt} - P_{0,y}^{tt}\right\| < \varepsilon_p$. If the condition is not satisfied, return to step (3).

(6) Verify annulus wellhead pressure: Compare whether the calculated and actual pressure of annulus wellhead satisfy $\|P_1^{tt} - P_c\| < \varepsilon_p$. If not, return to step (1);

(7) Drill string pressure calculation: Use the bottomhole pressure and the momentum conservation equation for the drill string to calculate the pressure at each node in the drill string.

(8) Update flow parameters and temperature: Update the flow parameters in the wellbore and calculate the temperature at node (y,r), $T_{(y,r)}^{tt}$. Verify whether $\left\|T_{(y,r)}^{tt} - T_{(y,r)}^{t(0)}\right\| < \varepsilon_T$. If the condition is not met, return to step (1) for recalibration.

(9) Pit gain verification: Calculate the pit gain at the current time and compare it with the critical detection value $V_{pg}^{tt} \geq V_c$. If satisfied, proceed to step (10); otherwise, move to the next time step and repeat steps (1) through (8).

(10) Well-killing adjustment: Set the bottomhole pressure P_b^{tt} to be slightly greater than the formation pore pressure P_p, and repeat steps (2) through (8) until the process is complete.

The overall calculation flow is shown in Fig. 3.

4. Results and analysis

A series of calculations were performed to demonstrate the advantages of the proposed model and to analyze the parameter response characteristics during well killing. For simplicity, it is assumed that the densities and viscosities of water- and oil-based drilling fluids are identical, and the rheological property of the well-killing fluid match that of the original drilling fluid. Pit gain is used as an indicator of gas kick. In practice, gas kick is typically detected when the pit gain reaches 1 m^3, allowing the well to be shut in promptly. However, during the shut-in process, formation gas may continue to invade the wellbore. To simplify the analysis, the model assumes that gas kick is detected and well-killing begins when the pit gain exceeds 3 m^3 or when gas is observed flowing out of the annulus wellhead, bypassing the shut-in process.

The simulated well is a vertical well with a gas kick originating at the bottomhole. The basic parameters of the simulated well are shown in Table 3.

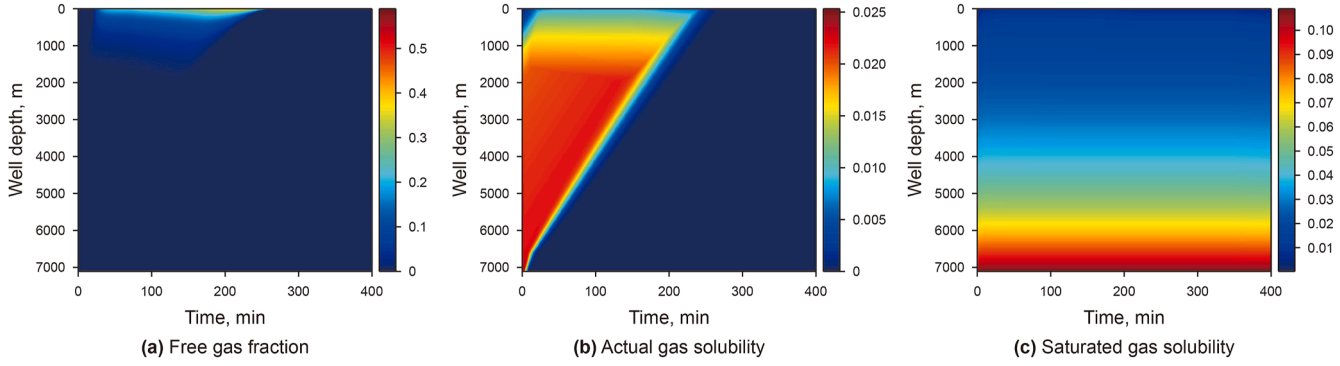

Fig. 5. Annulus gas migration in the oil-based drilling fluid.

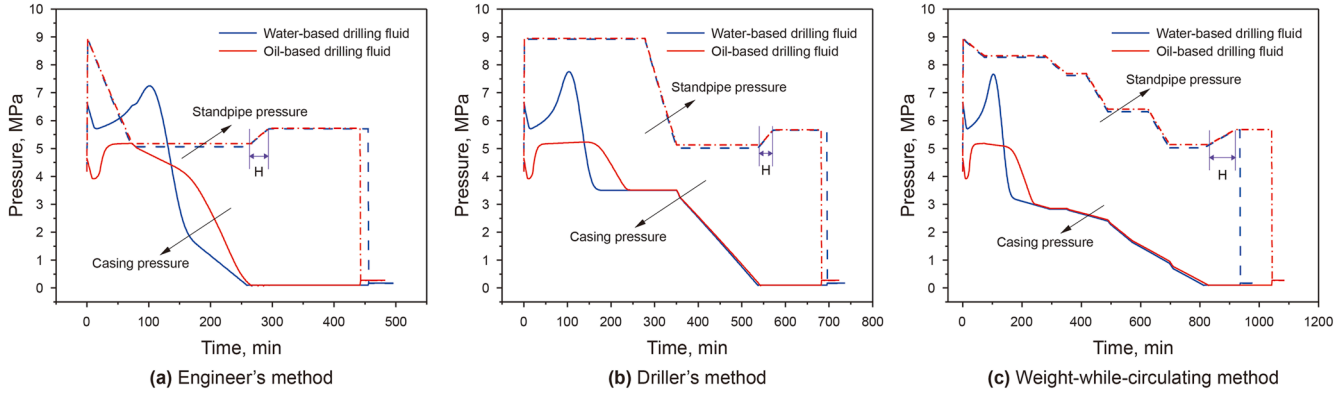

Fig. 6. Standpipe and casing pressures under various well-killing methods.

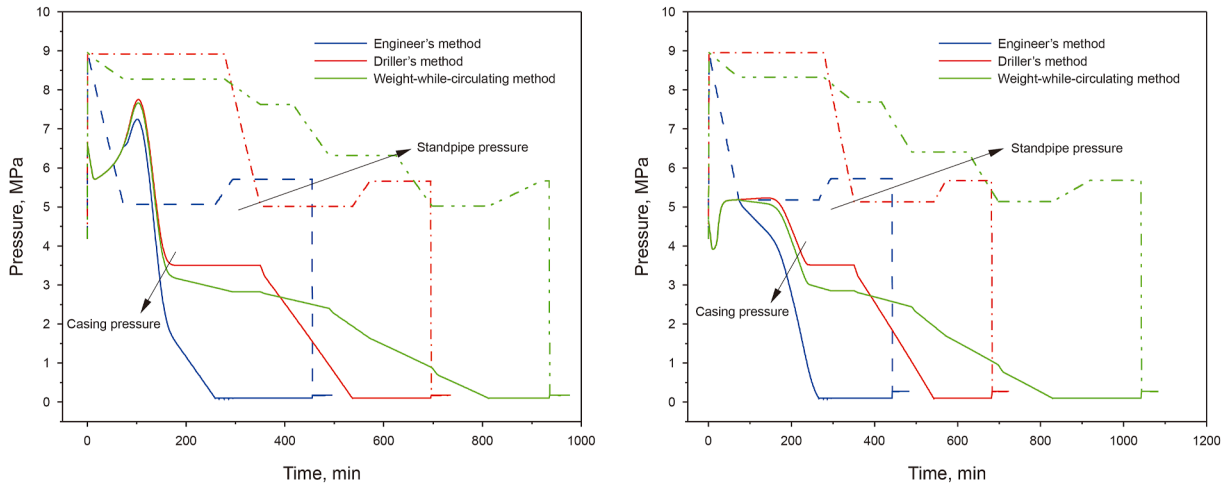

Fig. 7. Standpipe and casing pressures under different drilling fluids.

4.1. Annulus multiphase flow behavior during gas kick and well killing

Figs. 4 and 5 illustrate the gas migration patterns in the annulus during gas kick and well killing with water- and oil-based drilling fluids. The onset of the gas kick is set as time zero. The heavy muds of the driller's, engineer's, or weight-while-circulating methods influence casing pressure and gas migration behavior. Given the similarity in gas migration patterns among these methods, the driller's method is used as a representative case for analysis.

As shown in Fig. 4, under water-based drilling fluid condition, gas invasion into the annulus reaches approximately 2000 m with a maximum gas fraction of 10% from the onset of gas kick to the start of well killing. During outgassing, as the gas front remains below 2000 m, the gas fraction and distribution length increase slightly. However, once the gas front rises above 2000 m, the gas volume expansion rate accelerates, quickly reaching the wellhead. At this point, the maximum gas fraction reaches 32%. Therefore, during well killing, the greatest challenge occurs when gas is removing at the wellhead.

As shown in Fig. 5, under oil-based drilling fluid, gas remains dissolved below the depth of 1200 m due to the fluid's unsaturated state. Above this depth, the gas begins to separate out and expand.

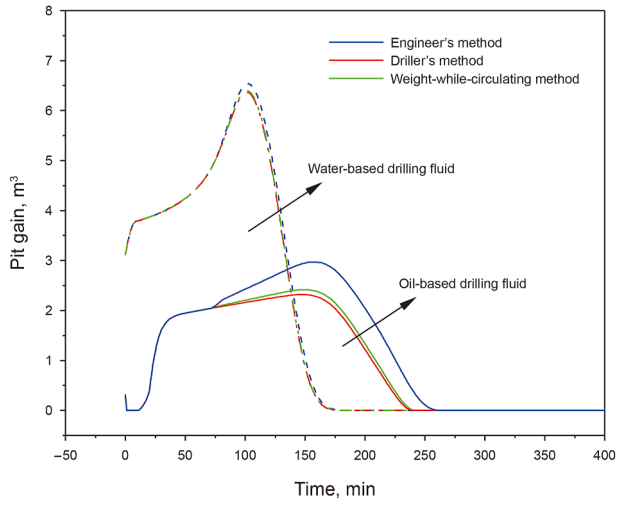

Fig. 8. Pit gain for various well-killing methods under different drilling fluids.

Unlike water-based drilling fluids, the gas kick under oil-based drilling fluid is detected when the gas reaches near the wellhead, where the gas fraction rapidly increases to 24%. During subsequent outgassing, the gas fraction at the wellhead remains stable, but the outgassing duration is longer than that under water-based fluid. Therefore, for oil-based drilling fluid, well control faces two key challenges: difficulty in early gas kick detection and the rapid increase in gas fraction at the wellhead, leaving insufficient time for well control preparation. However, if the gas kick is effectively managed upon detection, the complexity of subsequent well-killing operations is reduced.

4.2. Variations in key parameters for different well-killing methods

As mentioned above, the boundary matrix for each well-killing method can be defined according to its principles, enabling independent calculations for the engineer's method, driller's method, and weight-while-circulating method. Fig. 6 illustrates the variations in standpipe and casing pressures during well killing using water- and oil-based drilling fluids. The initial moment corresponds to the shut-in period before well killing begins. Although previous studies have analyzed the variations in standpipe and casing pressures during well killing (Zhang et al., 2012; Feng et al., 2015, 2016; Yuan et al., 2015), certain phenomena remain unexplored.

At the start of well killing, standpipe pressure quickly rises from the shut-in pressure to the initial circulating pressure and then varies based on the injection method of the well-killing fluid. The fluid density is typically designed for static wellbore condition during shut-in and is slightly larger than the equivalent density of the formation pore pressure. Therefore, combined with the circulating pressure loss, casing pressure drops to zero before the well-killing fluid reaches the annulus wellhead. If injection continues, bottomhole pressure exceeds the formation pore pressure and keeps rising, causing a gradual increase in standpipe pressure until the fluid is fully return to the annulus wellhead. This phenomenon, shown in section 'H' in Fig. 6, was overlooked in previous studies.

Under identical drilling fluid property conditions, standpipe pressures in oil- and water-based drilling fluids are consistent, but differences exist in casing pressure, primarily influenced by the gas flow state in the annulus. After well killing begins, annular pressure loss increase, causing casing pressure to initially decrease

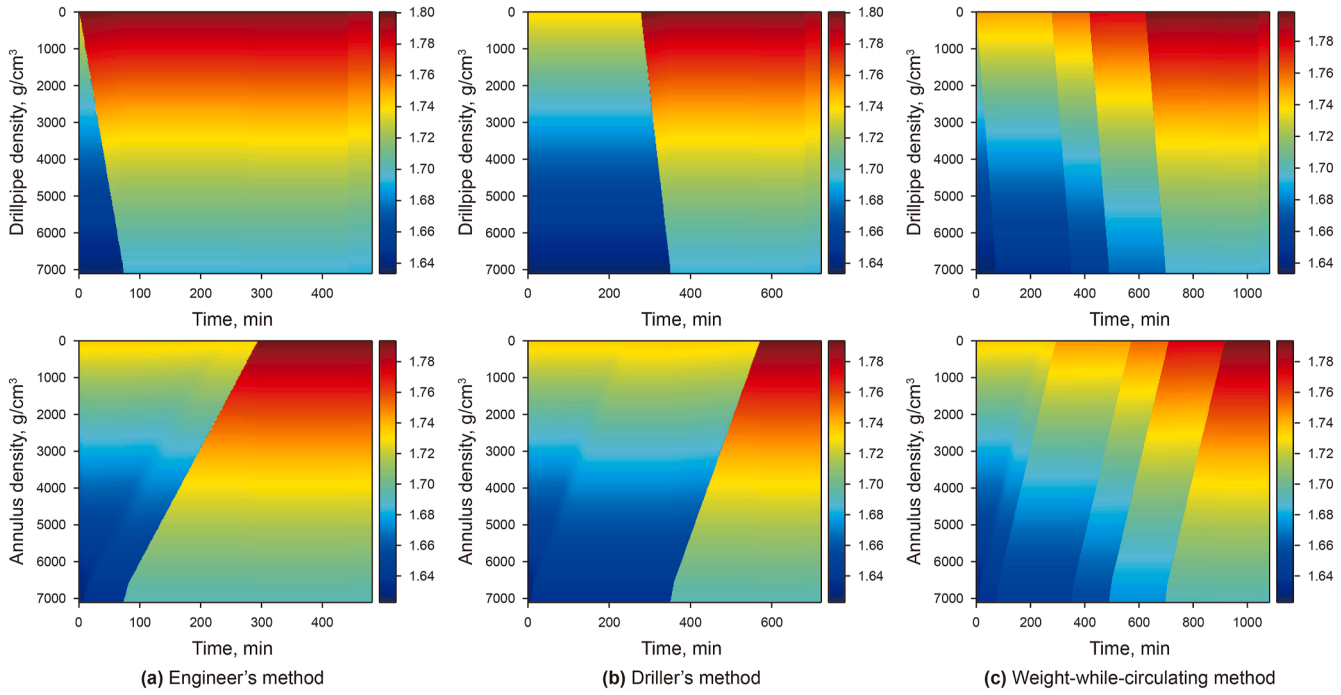

Fig. 9. Changes in fluid density in the drill string and annulus under different well-killing methods. The top is in the drill string and the bottom is in the annulus.

and then gradually rise. In water-based drilling fluid, as gas migrates toward the wellhead and rapidly expands, casing pressure increases sharply before decreasing, making control more challenging. In oil-based drilling fluid, due to gas dissolution and separation, casing pressure initially rises rapidly, then stabilizes, and eventually decreases. Before large gas remove out, casing pressure in oil-based drilling fluid is lower than that in water-based fluid, but the former outgassing takes longer. For both the driller's method and weight-while-circulating method, casing pressure changes in oil- and water-based fluids become identical once all gas is removed from the annulus. Upon completing the well-killing process and shutting in the well, both standpipe and casing pressures drop to atmospheric levels, signifying successful well-killing.

Maximum casing pressure and pit gain during well killing are critical parameters monitored by on-site engineers. The maximum casing pressure determines the choice of well-killing method and associated risks. Pit gain changes reflect the effectiveness of the operation. Fig. 7 compares the standpipe and casing pressure variations across different well-killing methods under various drilling fluid conditions. The engineer's method achieves the lowest maximum casing pressure and rapidly reduces both standpipe and casing pressures. However, the rapid pressure changes make it difficult to maintain stable casing pressure under annulus gas-liquid two-phase flow. The driller's method, by contrast, maintains high standpipe and casing pressures for an extended period, posing risks to surface equipment. During fluid injection, however, the single-phase wellbore flow facilitates easier control of casing pressure. The weight-while-circulating

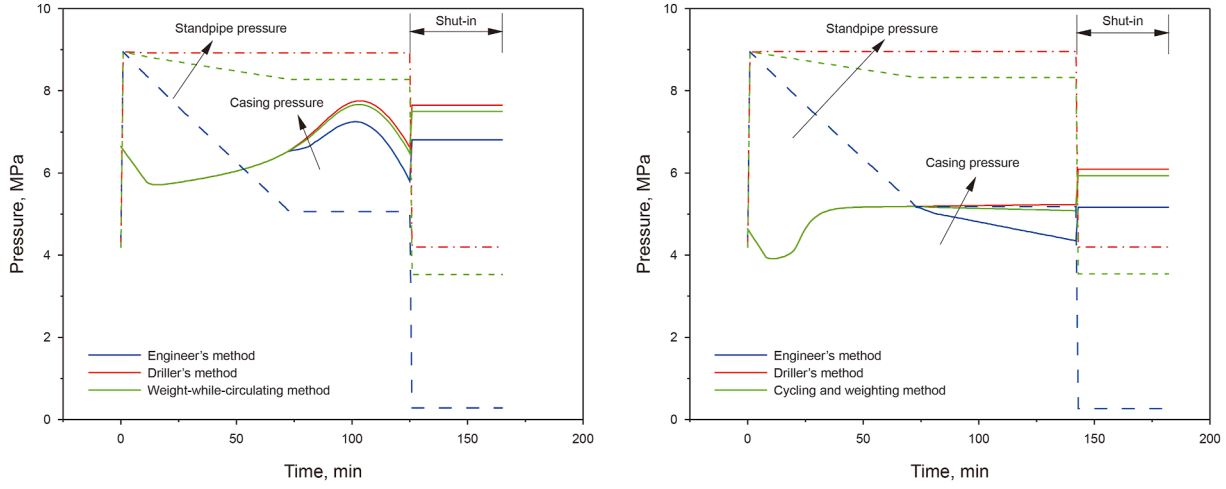

Fig. 10. Standpipe and casing pressures during well shut-in in water- and oil-based drilling fluids.

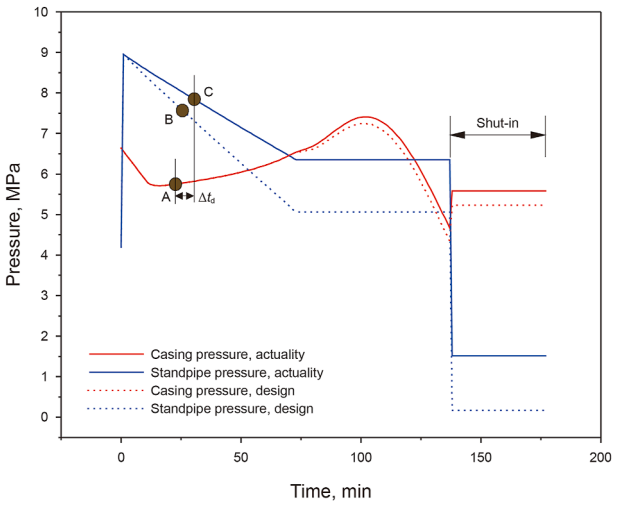

Fig. 11. Relationship between actual and designed pressures in a special scenario.

method moderately reduces standpipe and casing pressures, resulting in smoother pressure variations. Nevertheless, the presence of well-killing fluids with varying densities in the wellbore requires careful monitoring of their dynamic migration. The proposed model effectively addresses these challenges.

Fig. 8 illustrates the pit gain for various well-killing methods under different drilling fluids. The pit gain initially increases and then decreases to zero, consistent with field observations. This reflects the invading gas occupying the annular volume, leading to increased return flow of drilling fluid, followed by reinjection as the gas is discharged. Pit gain is larger with water-based drilling fluid than oil-based one due to gas dissolution effects. Earlier entry and higher density of well-killing fluid accelerate casing pressure reduction and increase gas expansion volume. The maximum pit gain follows the order: engineer's method > weight-while-circulating method > driller's method. Moreover, the wellbore structure and well-killing fluid density may cause notable differences in these values.

Fig. 9 shows the dynamic changes in fluid density and the migration of fluids with varying densities in the drill string and annulus under different well-killing methods. For the same drilling fluid, density decreases with increasing depth due to the combined effects of temperature and pressure. The distinct density line represents the leading fluid edge on the right and the trailing fluid edge on the left, with their movement over time reflecting fluid distribution and migration in the wellbore. Therefore, Fig. 9 enables dynamic tracking of key parameters such as the density, position, and height of well-killing fluids during different well-killing methods.

4.3. Determination of standpipe and casing pressures for well shut-in at any time

During well killing, standpipe pressure, casing pressure, outlet flow rate, and pit gain change dynamically. Due to the time delay in choke pressure wave propagation through the annulus and drill string, standpipe pressure changes do not correspond directly to casing pressure at the same moment. This makes it challenging to evaluate gas kick control solely by monitoring real-time parameters, especially during the outgassing phase. A practical solution is to periodically shut in the well during well killing and compare actual shut-in standpipe and casing pressures with theoretical values at the same time. To facilitate this, the model includes a function for calculating standpipe and casing pressures at any shut-in moment.

Fig. 10 shows the standpipe and casing pressures during well shut-in at a specific moment in water- and oil-based drilling fluids. Upon shut-in, the circulating pressure loss disappears, causing the standpipe pressure to decrease and the casing pressure to increase compared to the values immediately before shut-in. These changes are influenced by borehole parameters, drilling fluid properties, and pump rate. Before the well-killing fluid enters the annulus, the standpipe pressure differs obviously among the three well-killing methods under the same circulation time, with the shut-in standpipe pressure ranked as: driller's method > weight-while-circulating method > engineer's method. After the well-killing fluid enters the annulus, the engineer's method consistently results in the lowest shut-in standpipe and casing pressures, while the casing pressure relationship between the driller's method and the weight-while-circulating method depends on the circulating time.

Fig. 11 illustrates the relationship between actual and designed pressures when the density of the well-killing fluid used is lower than the designed density. During circulation, the actual and designed casing pressures are nearly identical, making it difficult to assess well-killing effectiveness. In contrast, the actual and designed standpipe pressures show a difference that increases over time. However, the standpipe pressure at a specific moment (point C) reflects the response to choke pressure from an earlier moment (point A), with a delay time (Δt_d) that depends on the gas fraction in the wellbore and is challenging to determine precisely.

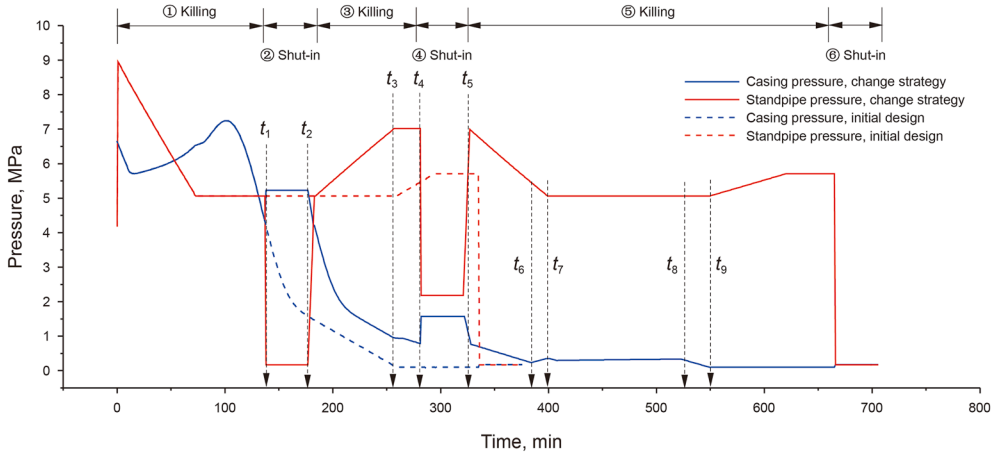

Fig. 12. Standpipe and casing pressures when the well-killing strategy is adjusted due to mud loss.

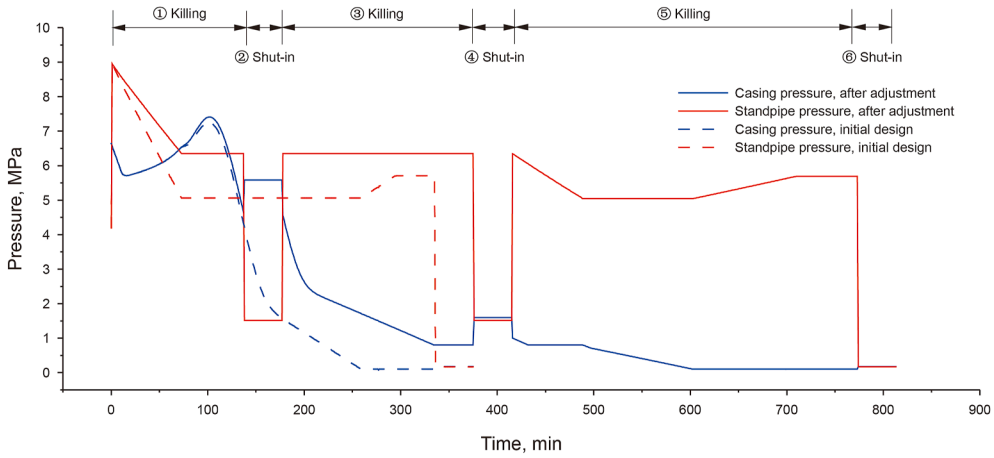

Fig. 13. Standpipe and casing pressures after adjusting the well-killing strategy due to low density of well-killing fluid.

Consequently, the actual standpipe pressure at point C may be misinterpreted as the designed standpipe pressure at an earlier moment (point B). Therefore, evaluating well-killing effectiveness based on standpipe pressure changes during circulation is unreliable. This scenario, while specific, reflects a general pattern in other cases (e.g., mud loss), where the differences between actual and designed pressures are either minimal or influenced by pressure propagation delays, making it similarly infeasible to judge well-killing effectiveness during circulation. After shutting in the well, however, the actual and designed pressures differ and represent values at the same moment. These differences can be used to determine whether the gas kick is effectively controlled and if other complications exist. It should be noted that the extent of these differences varies depending on the timing of the shut-in during well-killing.

4.4. Standpipe and casing pressures during temporary changes in well-killing strategy

Ultra-deep and complex formations are characterized by narrow safety density windows, extensive fractures and cavities, and high temperature and pressure. During well killing, various complications, such as secondary gas kick and mud loss, may arise, requiring adjustments to the well-killing strategy or parameters. The following two scenarios demonstrate the advantages of the model for handling temporary parameter adjustments.

Fig. 12 shows the standpipe and casing pressure curves when the well-killing strategy is adjusted due to insufficient well-killing fluid volume caused by mud loss. Initially, the engineer's method was employed with a well-killing fluid density of 1.80 g/cm^3 and a total volume of 250 m^3. The corresponding designed pressure curves are shown as dashed lines in Fig. 12. During the operation, 100 m^3 of well-killing fluid was lost, leaving only 100 m^3 in the annulus while the gas in the wellbore was not fully removed. To avoid excessive casing pressure due to prolonged shut-in, 70 m^3 of sealing fluid with a density of 1.77 g/cm^3 was prepared from the remaining 1.80 g/cm^3 fluid and injected. Simultaneously, an additional 250 m^3 of 1.80 g/cm^3 well-killing fluid was prepared. After injecting the 1.77 g/cm^3 fluid, the operation resumed with the newly prepared 1.80 g/cm^3 fluid until the well was successfully killed. Previous well-killing models struggled to account for such dynamic adjustments. However, the proposed model can modify and expand the original density and volume matrix (Eq. (65)) to recalculate standpipe and casing pressure curves for the revised strategy. The updated curves are shown as solid lines in Fig. 12.

$$F(\rho_L, V_L) = \left[1.8\ \mathrm{g/cm^3}, 250\ \mathrm{m^3}\right] \rightarrow F(\rho_L, V_L) = \begin{bmatrix} 1.80\ \mathrm{g/cm^3}, 100\ \mathrm{m^3} \\ 1.77\ \mathrm{g/cm^3}, 70\ \mathrm{m^3} \\ 1.80\ \mathrm{g/cm^3}, 250\ \mathrm{m^3} \end{bmatrix} \quad (65)$$

From the solid line in Fig. 12, it is evident that fluid loss was detected at t_1, leading to insufficient well-killing fluid. Then the well was shut in, and a well-killing fluid with a density of 1.77 g/cm^3 was prepared. Injection started at t_2 and ended at t_4. During this period, the fluid density decreased, causing the standpipe pressure to rise initially. When the well-killing fluid reached the bottomhole at t_3, the standpipe pressure stabilized. For safety, the well was briefly shut in from t_4 to t_5. Subsequently, the re-prepared well-killing fluid with a density of 1.80 g/cm^3 was injected. At t_7, this fluid reached the bit, resulting in a rapid decrease in standpipe pressure. At t_6, the original drilling fluid (1.75 g/cm^3) fully flow out of the wellbore, while the 1.80 g/cm^3 fluid in the drill string did not reach the bit, causing a slight increase in casing pressure between t_6 and t_7. At t_8, the 1.77 g/cm^3 fluid was discharged, and the injection of the 1.80 g/cm^3 fluid continued. During this phase, the casing pressure gradually decreased, reaching atmospheric pressure at t_9. The subsequent process followed the pattern shown in Fig. 6. This process demonstrates the complexity of fluid dynamics and pressure changes during well killing. The proposed model effectively captures key stages, showcasing its capability to handle such intricate scenarios with accuracy.

Fig. 13 shows the standpipe and casing pressure curves after adjusting the well-killing strategy due to the actual well-killing fluid density being lower than the designed value (Fig. 11), which resulted in a secondary gas kick. The initial strategy, based

Table 4
Basic parameters for Well #A and Well #B.

Parameter	Well #A	Well #B
Well depth of gas kick, m	8973	3447
Casing length, m	7881	3029
Casing inner diameter, m	0.197	0.225
Bit diameter, m	0.168	0.216
Drill pipe inner diameter, m	0.101	0.121
Drill pipe outer diameter, m	0.149	0.140
Well-killing pump rate, m^3/s	0.014	0.016→ 0.021 →0.025

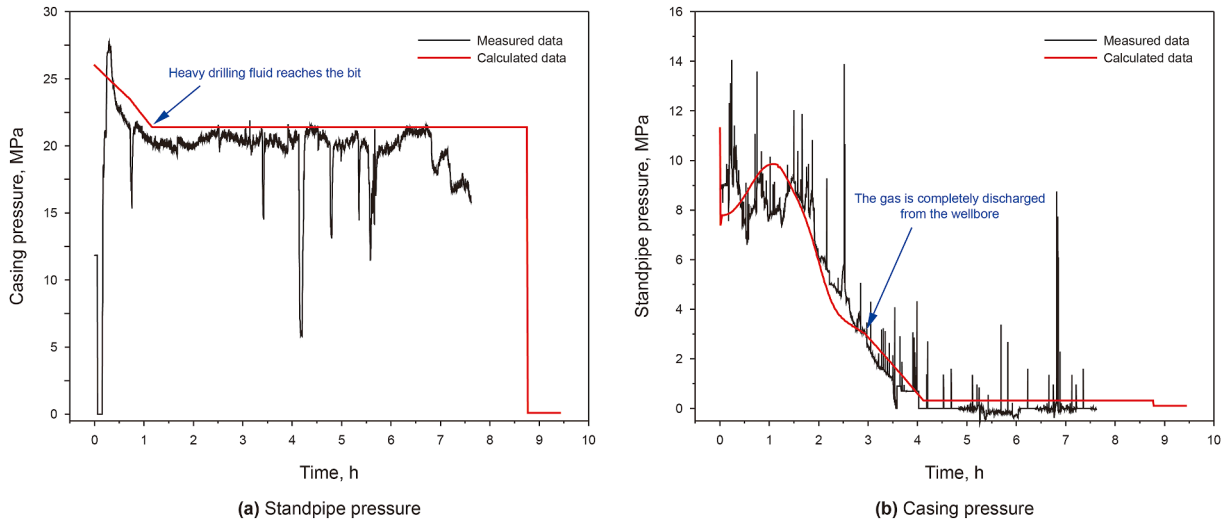

Fig. 14. Comparison of designed and actual well-killing pressure curves of Well #A.

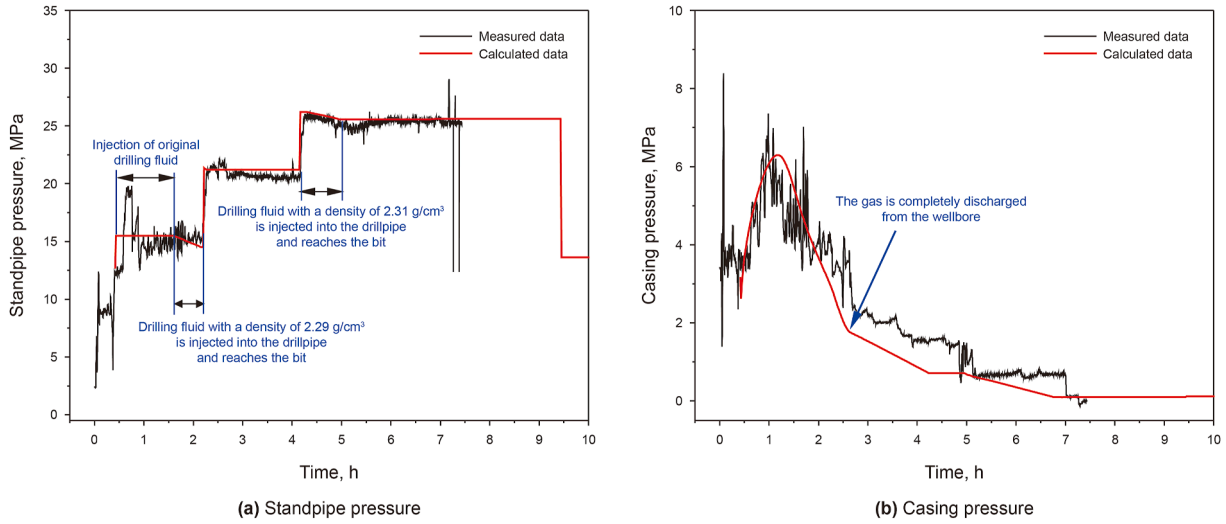

Fig. 15. Comparison of designed and actual well-killing pressure curves of Well #B.

on the engineer's method, specified a fluid density of 1.80 g/cm^3 and a volume of 250 m^3. However, due to configuration errors, the actual density was only 1.78 g/cm^3. Analysis shows that, after injecting 100 m^3 of well-killing fluid and shutting in the well, both the standpipe and casing pressures exceeded the designed values, triggering a secondary gas kick and necessitating a redesign of the well-killing parameters. Given the complexity of the wellbore conditions, directly increasing the fluid density to 1.80 g/cm^3 was infeasible. Therefore, the pseudo-driller's method was adopted: the gas was first removed using fluid with a density of 1.78 g/cm^3, followed by completion of the well-killing process with fluid at 1.80 g/cm^3. Eq. (66) outlines the modifications to the boundary matrix. Comparison of the initial and adjusted casing pressure curves indicates a longer circulation time after the secondary gas kick. The changes in standpipe and casing pressures are influenced by the dynamic flow of fluids with differing densities, and will not be analyzed in detail here.

$$F(\rho_L, V_L) = \left[1.8\ \mathrm{g/cm^3}, 250\ \mathrm{m^3}\right] \rightarrow F(\rho_L, V_L) = \begin{bmatrix} 1.78\ \mathrm{g/cm^3}, 100\ \mathrm{m^3} \\ 1.78\ \mathrm{g/cm^3}, 150\ \mathrm{m^3} \\ 1.80\ \mathrm{g/cm^3}, 250\ \mathrm{m^3} \end{bmatrix} \tag{66}$$

Another scenario in ultra-deep formation well-killing involves designing well-killing parameters by incorporating multiple methods to address challenges such as high casing pressure and inaccuracies in formation pore pressure prediction. Simulations using this model align with the results described above, with the only distinction being the need for a pre-designed boundary matrix, which is not discussed here. Notably, this scenario is difficult to addressed using conventional models.

5. Case studies

To further verify the applicability and reliability of this model, field tests were conducted on two onshore directional wells. Well #A utilized a water-based drilling fluid, while Well #B employed an oil-based drilling fluid. Considering the high-risk nature of well-killing operations, the engineer's method was applied to Well #A, and a combination of the driller's method and the weight-while-circulating method was used for Well #B. The basic parameters for both wells are summarized in Table 4.

Well #A encountered a gas kick while drilling at 8973 m in the vertical section. The pit gain was 1.5 m^3, with a shut-in standpipe pressure of 5 MPa and a shut-in casing pressure of 11.3 MPa. The engineer's method was employed to handle the situation, directly increasing the drilling fluid density from 1880 to 1940 kg/m^3.

During drilling to a depth of 3447 m in the vertical section, Well #B experienced an overflow, resulting in a pit gain of 0.45 m^3, a shut-in standpipe pressure of 2.1 MPa, and a shut-in casing pressure of 3.15 MPa. A combination of the driller's method and the weight-while-circulating method was employed. Initially, drilling fluid with a density of 2250 kg/m^3 was used for outgassing. The killing fluid density was then increased to 2290 kg/m^3 for weighting, and the well was ultimately killed with killing fluid at a density of 2310 kg/m^3.

For Well #A, the two-phase flow model during a gas kick indicated that a pit gain of 1.5 m^3 was insufficient to raise the shut-in casing pressure to 11.3 MPa, suggesting continued gas kick during shut-in. The bottomhole gas kick volume was corrected based on the shut-in casing pressure, resulting in a true pit gain of 3.6 m^3. The standpipe and casing pressure curves for well-killing were then calculated (Fig. 14) and used to guide the operation. The well-killing process proceeded without complications, and the designed pressure curves closely aligned with the actual construction curves, verifying the model's reliability under water-based drilling fluid.

For Well #B, gas migration to the wellhead was detected with a pit gain of only 0.45 m^3, and the shut-in casing pressure remained below 3.15 MPa. Using the gas-liquid two-phase flow model that accounts for gas dissolution in oil-based drilling fluid, the bottomhole gas kick rate and volume were recalculated, corresponding to a corrected pit gain of 1.42 m^3. Based on this correction, standpipe and casing pressure curves were designed for the well-killing operation. During the process, pump rates were adjusted twice, requiring redesigns of the pressure curves, as shown in Fig. 15. The well-killing operation proceeded without complications, and the designed pressure curves closely matched the actual construction data, validating the model's applicability to oil-based drilling fluids.

6. Conclusion

This paper establishes a dynamic unified well-killing model to synergistically regulate multiple choke-while-circulating well-killing methods. The wellhead pressure responses of the driller's, engineer's, and weight-while-circulating methods, both individually and in combination, are analyzed. The main conclusions are as follows:

(1) During well killing, as annulus gas migrates to the wellhead, gas expansion and separation sharply increase the gas flow rate and volume fraction, presenting the greatest control challenge. The maximum casing pressure is lower with oil-based drilling fluid than with water-based one, but the gas discharge duration is longer.

(2) During well killing, casing pressure may drop to zero before well-killing fluid reaches the annulus wellhead. Continued injection can cause bottomhole pressure to exceed pore pressure, leading to a gradual increase in standpipe pressure. This phenomenon, often overlooked in previous studies, should be accounted for when controlling well killing based on standpipe pressure.

(3) This model overcomes the challenges of calculating scenarios involving combined well-killing methods or temporary strategy changes by requiring only real-time updates to the boundary matrix. Key parameters, such as pit gain, wellhead pressures, and the density, position, and height of wellbore fluids, can be dynamically monitored.

(4) Field applications in two wells using water- and oil-based drilling fluids demonstrated good consistency between the designed and actual construction curves, verifying the model's reliability and applicability.

CRediT authorship contribution statement

Hong-Wei Yang: Writing – original draft, Supervision, Methodology, Conceptualization. **Jun Li:** Writing – review & editing, Supervision, Conceptualization. **Zhen-Yu Long:** Visualization, Supervision. **Xiu-Ling Zhang:** Supervision. **Geng Zhang:** Supervision. **Hui Zhang:** Writing – review & editing. **Re-Yu Gao:** Data curation.

Declaration of competing interest

The authors declare that they have no known competing financial interests or personal relationships that could have appeared to influence the work reported in this paper.

Acknowledgments

This paper is supported by the National Natural Science Foundation of China (52474018, 52227804, U22B2072, 52404012), the National Key Research and Development Program of China (2023YFC3009200), and the Science Foundation of China University of Petroleum, Beijing (2462023BJRC008, 2462024XKBH006).

References

Ansari, A.M., Sylvester, N.D., Sarica, C., et al., 1994. A comprehensive mechanistic model for upward two-phase flow in wellbores. SPE Prod. Facil. 9 (2), 143–151. https://doi.org/10.2118/20630-PA.

Beggs, D.H., Brill, J.P., 1973. A study of two-phase flow in inclined pipes. J. Petrol. Technol. 25 (5), 607–617. https://doi.org/10.2118/4007-PA.

Bjørkevoll, K.S., Skogestad, J.O., Frøyen, J., et al., 2018. Well control simulator: enhancing models with compositional PVT models and kinetics. In: The IADC/SPE Drilling Conference and Exhibition. https://doi.org/10.2118/189651-MS.

Chantose, P., Oskarsen, R., Emilsen, M., et al., 2018. Dynamic kill method using staged fluid densities can improve the kill ability of relief Wells for challenging blowouts. In: The IADC/SPE Drilling Conference and Exhibition. https://doi.org/10.2118/189655-MS.

Davoudi, M., Smith, J.R., Patel, B.M., et al., 2011. Evaluation of alternative initial responses to kicks taken during managed-pressure drilling. SPE Drill. Complet. 26 (2), 169–181. https://doi.org/10.2118/128424-PA.

Espinosa-Paredes, G., Espinosa-Martínez, E.G., 2009. A feedback-based inverse heat transfer method to estimate unperturbed temperatures in wellbores. Energy Convers. Manag. 50 (1), 140–148. https://doi.org/10.1016/j.enconman.2008.08.017.

Feng, J., Fu, J., Chen, P., et al., 2015. Predicting pressure behavior during dynamic kill drilling with a two-phase flow. J. Nat. Gas Sci. Eng. 22, 591–597. https://doi.org/10.1016/j.jngse.2015.01.006.

Feng, J., Fu, J., Chen, P., et al., 2016. An advanced Driller's method simulator for deepwater well control. J. Loss Prev. Process. Ind. 39, 131–140. https://doi.org/10.1016/j.jlp.2015.11.026.

Gao, Y., Sun, B., Xu, B., et al., 2017. A wellbore/formation-coupled heat-transfer model in deepwater drilling and its application in the prediction of hydrate-

reservoir dissociation. SPE J. 22 (3), 756–766. https://doi.org/10.2118/184398-PA.
Grimstad, A.A., Linga, H., Haave, Ø., et al., 2017. Degassing rate of drilling fluid base oils as exposed to depressurisation and drill string rotation. In: The SPE/IADC Drilling Conference and Exhibition. https://doi.org/10.2118/184707-MS.
Goins, Jr, W.C., 1969. Blowout Prevention. Practical Drilling Technology. United States: N. Web. https://www.osti.gov/biblio/6811028.
Hasan, A.R., Kabir, C.S., 1988. A study of multiphase flow behavior in vertical Wells. SPE Prod. Eng. 3 (2), 263–272. https://doi.org/10.2118/15138-PA.
He, D., Jia, C., Zhao, W., et al., 2023. Research progress and key issues of ultra-deep oil and gas exploration in China. Petrol. Explor. Dev. 50 (6), 1333–1344. https://doi.org/10.1016/S1876-3804(24)60470-2.
Holand, P., 2001. Reliability of deepwater subsea blowout preventers. SPE Drill. Complet. 16 (1), 12–18. https://doi.org/10.2118/70129-PA.
Johnson, A., Piccolo, B., Pinkstone, H., et al., 2017. Augmenting deepwater well control with managed pressure drilling equipment. In: The SPE/IATMI Asia Pacific Oil & Gas Conference and Exhibition. https://doi.org/10.2118/186331-MS.
Ju, G.S., Yan, T., Sun, X.F., et al., 2022. Evolution of gas kick and overflow in wellbore and formation pressure inversion method under the condition of failure in well shut-in during a blowout. Pet. Sci. 19 (2), 678–687. https://doi.org/10.1016/j.petsci.2022.01.004.
Letbetter, S.C., 1975. Kick detection and well control training. In: The SPE California Regional Meeting. https://doi.org/10.2118/5353-MS.
Li, L., Xu, X., Zhu, J., et al., 2016. Application of Innovative high-temperature high-density Oil-based Drilling Fluid Technology in the Efficient Exploration and Development of Ultra-deep Natural Gas Resources in West China. The International Petroleum Technology Conference. https://doi.org/10.2523/IPTC-18600-MS.
Ma, Y., Cai, X., Yun, L., et al., 2022. Practice and theoretical and technical progress in exploration and development of Shunbei ultra-deep carbonate oil and gas field, Tarim Basin, NW China. Petrol. Explor. Dev. 49 (1), 1–20. https://doi.org/10.1016/S1876-3804(22)60001-6.
Ma, Z., Vajargah, A.K., Ambrus, A., et al., 2016. Multi-phase well control analysis during managed pressure drilling operations. In: The SPE Annual Technical Conference and Exhibition. https://doi.org/10.2118/181672-MS.
Mao, G., Zhang, J., 2025. Research on dynamic well control in riserless mud recovery system. Process Saf. Environ. Prot. 193, 205–216. https://doi.org/10.1016/j.psep.2024.10.125.
Meng, Y., Xu, C., Wei, N., et al., 2015. Numerical simulation and experiment of the annular pressure variation caused by gas kick/injection in wells. J. Nat. Gas Sci. Eng. 22, 646–655. https://doi.org/10.1016/j.jngse.2015.01.013.
Monteiro, E.N., Ribeiro, P.R., Lomba, R.F., 2008. Study of the PVT properties of gas-synthetic drilling fluid mixtures applied to well control. SPE Annual Technical. Exhib. https://doi.org/10.2118/116013-MS.
Nickens, H.V., 1987. A dynamic computer model of a kicking well. SPE Drill. Eng. 2 (2), 159–173. https://doi.org/10.2118/14183-PA.
Noynaert, S.F., Schubert, J.J., 2005. Modeling ultra-deepwater blowouts and dynamic kills and the resulting blowout control best practices recommendations. SPE/IADC Drilling Conference. https://doi.org/10.2118/92626-MS.
Nunes, J.O.L., Bannwart, A.C., Ribeiro, P.R., 2002. Mathematical modeling of gas kicks in deep water scenario. IADC/SPE Asia Pacific Drilling Technol. https://doi.org/10.2118/77253-MS.
Nwaka, N., Wei, C., Chen, Y., 2020. A simplified two-phase flow model for riser gas management with non-aqueous drilling fluids. J. Energy Resour. Technol. 142 (10), 103001. https://doi.org/10.1115/1.4046774.
O'bryan, P.L., 1998. Well control problems associated with gas solubility in oil-based drilling fluids. PhD Dissertation. Louisiana State University.
Orkiszewski, J., 1967. Predicting two-phase pressure drops in vertical pipe. J. Petrol. Technol. 19 (6), 829–838. https://doi.org/10.2118/1546-PA.
Petersen, J., Rommetveit, R., Bjørkevoll, K.S., et al., 2008. A general dynamic model for single and multi-phase flow operations during drilling, completion, well control and intervention. IADC/SPE Asia Pacific Drilling Technol. Con. Exhib. https://doi.org/10.2118/114688-MS.
Rommetveit, R., Blyberg, A., Olsen, T.L., 1989. The effects of operating conditions, Reservoir characteristics and control methods on gas kicks in oil based drilling muds. In: The SPE Offshore Europe. https://doi.org/10.2118/19246-MS.
Santos, H., Catak, E., Kinder, J.O.E., et al., 2007. Kick detection and control in oil-based mud: real well-test results using microflux control equipment. In: The SPE/IADC Drilling Conference. https://doi.org/10.2118/105454-MS.
Shi, H., Holmes, J.A., Durlofsky, L.J., et al., 2005. Drift-flux modeling of two-phase flow in wellbores. SPE J. 10 (1), 24–33. https://doi.org/10.2118/84228-PA.
Su, Y., Ma, H., Guo, J., et al., 2024. The behaviors of gas-liquid two-phase flow under gas kick during horizontal drilling with oil-based muds. Petroleum 10 (1), 49–67. https://doi.org/10.1016/j.petlm.2023.10.002.
Sun, B., Sun, X., Wang, Z., et al., 2017. Effects of phase transition on gas kick migration in deepwater horizontal drilling. J. Nat. Gas Sci. Eng. 46, 710–729. https://doi.org/10.1016/j.jngse.2017.09.001.
Sun, B., Guo, Y., Sun, W., et al., 2018a. Multiphase flow behavior for acid-gas mixture and drilling fluid flow in vertical wellbore. J. Petrol. Sci. Eng. 165, 388–396. https://doi.org/10.1016/j.petrol.2018.02.016.
Sun, B., Fu, W., Wang, N., et al., 2019. Multiphase flow modeling of gas intrusion in oil-based drilling mud. J. Petrol. Sci. Eng. 174, 1142–1151. https://doi.org/10.1016/j.petrol.2018.12.018.
Sun, X., Sun, B., Zhang, S., et al., 2018b. A new pattern recognition model for gas kick diagnosis in deepwater drilling. J. Petrol. Sci. Eng. 167, 418–425. https://doi.org/10.1016/j.petrol.2018.04.035.
Thomas, D.C., Lea Jr, J.F., Turek, E.A., 1984. Gas solubility in oil-based drilling fluids: effects on kick detection. J. Petrol. Technol. 36 (6), 959–968. https://doi.org/10.2118/11115-PA.
Vega, M.P., Fernandes, L.D., de Moraes Oliveira, G.F., et al., 2025. Gas kick dynamic circulation in MPD operations with water based drilling fluid: maximum casing pressure modeling and validation. Geoenergy Sci. Eng. 244, 213437. https://doi.org/10.1016/j.geoen.2024.213437.
Wang, Z., Sun, B., 2009. Annular multiphase flow behavior during deep water drilling and the effect of hydrate phase transition. Pet. Sci. 6, 57–63. https://doi.org/10.1007/s12182-009-0010-3.
Wei, N., Meng, Y., Li, G., et al., 2014. Transient flow characteristics of gas lift in underbalanced drilling. Acta Pet. Sin. 35 (1), 166–171. https://www.syxb-cps.com.cn/EN/10.7623/syxb201401021.
Wei, N., Xu, C., Meng, Y., et al., 2018. Numerical simulation of gas-liquid two-phase flow in wellbore based on drift flux model. Appl. Math. Comput. 338, 175–191. https://doi.org/10.1016/j.amc.2018.03.067.
White, D.B., Walton, I.C., 1990. A computer model for kicks in water-and oil-based muds. In: The IADC/SPE Drilling Conference. https://doi.org/10.2118/19975-MS.
Xu, C., Meng, Y., Wei, N., et al., 2015. Experimental simulation and numerical modeling of dynamic variations in wellbore pressure during gas-kicks. Acta Pet. Sin. 36 (1), 120–126. https://www.syxb-cps.com.cn/EN/10.7623/syxb201501015.
Xu, Z., Chen, X., Song, X., et al., 2021. Gas-kick simulation in oil-based drilling fluids with nonequilibrium gas-dissolution and-evolution effects. SPE J. 26 (5), 2549–2569. https://doi.org/10.2118/206717-PA.
Yang, H., Li, J., Liu, G., et al., 2019a. A transient hydro-thermo-bubble model for gas kick simulation in deep water drilling based on oil-based mud. Appl. Therm. Eng. 158, 113776. https://doi.org/10.1016/j.applthermaleng.2019.113776.
Yang, H., Li, J., Liu, G., et al., 2019b. Numerical analysis of transient wellbore thermal behavior in dynamic deepwater multi-gradient drilling. Energy 179, 138–153. https://doi.org/10.1016/j.energy.2019.04.214.
Yang, H., Li, J., Liu, G., et al., 2020. The effect of interfacial mass transfer of slip-rising gas bubbles on two-phase flow in the vertical wellbore/pipeline. Int. J. Heat Mass Tran. 150, 119326. https://doi.org/10.1016/j.ijheatmasstransfer.2020.119326.
Yang, H.W., Li, J., Jiang, J.W., et al., 2022. A dynamic managed pressure well-control method for rapid treatment of gas kick in deepwater managed pressure drilling. Pet. Sci. 19 (5), 2297–2313. https://doi.org/10.1016/j.petsci.2022.06.011.
Yang, M., Li, X., Deng, J., et al., 2015. Prediction of wellbore and formation temperatures during circulation and shut-in stages under kick conditions. Energy 91, 1018–1029. https://doi.org/10.1016/j.energy.2015.09.001.
Yang, Z., Ye, C., Wang, Q., et al., 2024. Pore pressure prediction in deep complex formations based on well-seismic combination. In: The 58th U.S. Rock Mechanics/Geomechanics Symposium. https://doi.org/10.56952/ARMA-2024-0758.
Yin, B., Liu, G., Li, X., 2017. Multiphase transient flow model in wellbore annuli during gas kick in deepwater drilling based on oil-based mud. Appl. Math. Model. 51, 159–198. https://doi.org/10.1016/j.apm.2017.06.029.
Yin, B., Pan, S., Zhang, X., et al., 2022. Effect of oil viscosity on flow pattern transition of upward gas-oil two-phase flow in vertical concentric annulus. SPE J. 27 (6), 3283–3296. https://doi.org/10.2118/210585-PA.
Yin, B., Ren, M., Liu, S., et al., 2023. Dynamic well killing method based on Y-tube principle when the drill bit is off-bottom. Eng. Sci. Technol. Inter. J. 41, 101385. https://doi.org/10.1016/j.jestch.2023.101385.
Yin, B., Ding, T., Zhang, X., et al., 2024a. Pressure drop predicting model for gas and oil-based drilling fluid two phase flow in vertical annulus. Microgravity Sci. Technol. 36 (1), 8–18. https://doi.org/10.1007/s12217-023-10090-9.
Yin, H., Li, G., Xiao, J., et al., 2024b. Intelligent inversion analysis of drilling gas kick characteristic parameters and advanced predictions of development trends. SPE J. 29 (6), 2953–2970. https://doi.org/10.2118/219474-PA.
Yin, H., Cui, H., Li, Q., et al., 2025. Numerical analysis of managed pressure relief during shut-in periods after gas kicks in multi-pressure formations. Geoenergy Sci. Eng. 246, 213619. https://doi.org/10.1016/j.geoen.2024.213619.
Yuan, Z., Hashemian, Y., Morrell, D., 2015. Ultra-deepwater blowout well control analysis under worst case blowout scenario. J. Nat. Gas Sci. Eng. 27, 122–129. https://doi.org/10.1016/j.jngse.2015.08.047.
Zhang, R., Li, J., Liu, G., et al., 2021. The coupled model of wellbore temperature and pressure for variable gradient drilling in deep water based on dynamic mass flow. J. Petrol. Sci. Eng. 205, 108739. https://doi.org/10.1016/j.petrol.2021.108739.
Zhang, Z., Xiao, T., Fu, J., 2012. Study on well-kill calculation model with deep-water engineer's method. Adv. Mater. Res. 393, 996–999. https://doi.org/10.4028/www.scientific.net/AMR.393-395.996.
Zhang, Z., Sun, B., Wang, Z., et al., 2022. Intelligent well killing control method driven by coupling multiphase flow simulation and real-time data. J. Petrol. Sci. Eng. 213, 110337. https://doi.org/10.1016/j.petrol.2022.110337.
Zhou, H., Sun, M., Niu, X., et al., 2018. A novel multi-density dynamic well killing method for ultra-deep Wells and the simulation system. In: The Abu Dhabi International Petroleum Exhibition & Conference. https://doi.org/10.2118/193216-MS.